

Controlling Molecular Conformation for Highly Efficient and Stable Deep-Blue Copolymer Light-Emitting Diodes

*Iain Hamilton,[†] Nathan Chander,[†] Nathan J. Cheetham,[†] Minwon Suh,[†] Matthew Dyson,^{†,§}
Xuhua Wang,[†] Paul N. Stavrinou,[‡] Michael Cass,[⊥] Donal D. C. Bradley,^{*,‡,||} and Ji-Seon Kim^{*,†}*

[†] Department of Physics and Centre for Plastic Electronics, Imperial College London, London SW7 2AZ, UK

[‡] Department of Engineering Science, University of Oxford, Parks Road, Oxford, OX1 3PJ, UK

[§] Molecular Materials and Nanosystems and Institute for Complex Molecular Systems, Eindhoven University of Technology, P.O. Box 513, 5600 MB Eindhoven, The Netherlands

[⊥] Cambridge Display Technology Ltd, Unit 12 Cardinal Park, Godmanchester, Cambridgeshire PE29 2XG, UK

^{||} Department of Physics and Division of Mathematical, Physical and Life Sciences, University of Oxford, 9 Parks Road, Oxford, OX1 3PD, UK

KEYWORDS: deep-blue, polymer light-emitting diodes, β -phase, polyfluorenes, copolymers

ABSTRACT

We report a novel approach to the achievement of deep-blue, high-efficiency, and long-lived solution processed polymer light-emitting diodes (PLEDs) via a simple molecular-level conformation change whereby we introduce rigid β -phase segments into a 95% fluorene - 5% arylamine copolymer emission layer (EML). The arylamine moieties at low density act as efficient exciton formation sites in PLEDs whilst the conformational change alters the nature of the dominant luminescence from a broad, charge-transfer like emission to a significantly blue-shifted and highly vibronically structured, excitonic emission. As a consequence, we observe a significant improvement in Commission International de L'Eclairage (CIE) (x, y) co-ordinates from (0.149, 0.175) to (0.145, 0.123) whilst maintaining high efficiency and improving stability. We achieve peak luminous efficiency, $\eta = 3.60$ cd/A and luminous power efficiency, $\eta_w = 2.44$ lm/W; values that represent state of the art performance for single copolymer deep-blue PLEDs. These values are five-fold better than for otherwise-equivalent, β -phase poly(9,9-dioctylfluorene) (PFO) EML PLEDs (0.70 cd/A and 0.38 lm/W). This report represents the first demonstration of the use of molecular conformation as a vector to control the optoelectronic properties of a fluorene copolymer; previous examples have been confined to homopolymers.

INTRODUCTION

Since the discovery of electroluminescence from conjugated polymers in 1989,¹ there has been significant interest in solution processable PLEDs as potential candidates for low cost, energy efficient display and lighting applications. Tremendous efforts have been made to develop deep-blue (usually defined by the electroluminescence (EL) emission having CIE (x, y) coordinates both ≤ 0.15)² light emitting polymers (LEPs) for use in high-luminance and high-efficiency PLED displays,^{3–5} with this requirement essential to achieving the colour gamut needed for high quality display applications. An additional commercialisation challenge is the limited stability of blue fluorescent LEPs,⁶ for which the operational device lifetime is relatively short compared to red and green phosphorescence-based polymer emitters; the latter have encapsulated lifetimes of over 100,000 hours.⁷ In this paper we report a novel approach to the achievement of deep-blue, high-efficiency, and long-lived PLEDs via the introduction of a conformation change in the conjugated backbone of a fluorene-arylamine copolymer.

Conjugated polymers based on fluorene backbones have been extensively studied as blue OLED emission materials on account of both (i) their wide optical gaps, e.g. ~ 3.0 eV for PFO,⁸ that are favourable for deep-blue emission and (ii) their high photoluminescence (PL) quantum yields, e.g. up to 50-60% for glassy phase poly(9,9-di-octylfluorene) (PFO) (see Figure 1(a)).^{9,10} They can, however, suffer from poor operational and colour stability arising from fluorenone defects, giving rise to ‘green band’ excimer emission at 535 nm.^{11–13} PFO is an especially well-studied member of the fluorene-homopolymer family and can be prepared with a number of distinct microstructures^{14,15}, namely the glassy-,^{14–16} crystalline-,^{14,15,17,18} liquid-crystalline (LC)^{15,19–21} and chain-segment-extended β -phases.^{14,15,22–26} The β -phase has an increased

backbone planarity within a fraction of chain segments, with the corresponding torsion angle between adjacent fluorene units $\approx 180^\circ$, resulting in the octyl substituent groups for neighbouring monomers lying on opposite sides of the chain. In contrast, the glassy phase is a disordered phase with a broad distribution of torsion angles between monomers.^{14–16} The different phases can be identified using both optical absorption and PL spectroscopy measurements.^{14,21,25–28}

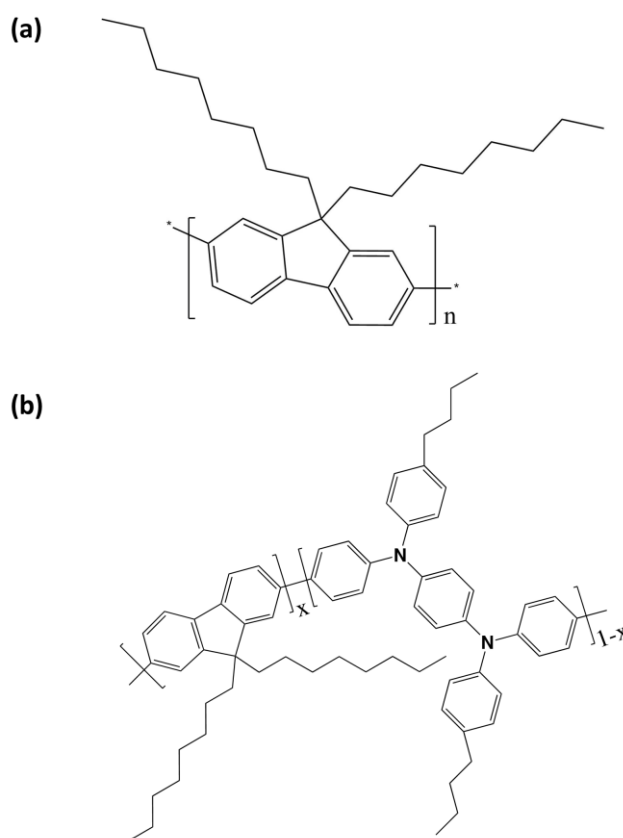


Figure 1. Chemical structures for (a) poly(9,9-dioctylfluorene) (100F8 or PFO) and (b) 9,9-dioctylfluorene:butyl substituted phenylenediamine (F8:BSP) copolymers ($x = 0.97, 0.95, 0.90, 0.80$ for 97F8:3BSP, 95F8:5BSP, 90F8:10BSP, 80F8:20BSP and $x = 0.50$ for 50F8:50BSP or PFB).

The β -phase has attracted much attention due to the action of its extended chain segments as a ‘self-dopant’²⁰ within an otherwise glassy matrix. These segments constitute the most ordered,

lowest energy states and trigger an efficient energy transfer from the surrounding high energy state glassy segments.^{14,20,22,27,28} The β -phase chain segments have been shown to act as charge carrier-trapping and exciton formation sites, with the extension in conjugation length reducing the optical gap of PFO by some 0.3 eV.^{20,24,27,29–32} As a consequence, β -phase PFO PLEDs have been reported with a nearly two-fold increase in luminous efficiency from 1.0 cd/A to 1.9 cd/A compared to their glassy counterparts.^{30,33} As yet such an approach has not been applied to copolymers. Finally, there are numerous processing methods by which to induce β -phase chain segments, with reported methods including (i) thermal cycling,^{20,21,34} (ii) Langmuir-Bodgett film formation and transfer,³⁵ (iii) deposition of films from mixed solvent,²³ solvent/additive³³ and high boiling point solvent²⁸ solutions, (iv) post-deposition film exposure to solvent vapours,²¹ and (v) dipping in/flooding with solvent.^{23,30}

Approaches to high efficiency within simple PLED device architectures require that individual layers be optimized to perform more than one function. In contrast to blending materials with different functionality³⁶, covalently linked copolymers combine functionalities in a way that is resistant to phase separation. As a consequence, state of the art polymer LED emission materials are now invariably complex copolymers featuring emission and electron- and hole-transport moieties with optimized fractional compositions and chain architectures.^{37–39} In this study we focus on 9,9-dioctylfluorene (F8):butyl-substituted phenylenediamine (BSP) copolymers (see Figure 1(b)) and in particular the 95% F8:5% BSP, or for short 95F8:5BSP, copolymer. During synthesis, the insertion of BSP units into each copolymer chain is subject to the constraint that since BSP-BSP couplings are not possible (see experimental section below for further details) each BSP unit must have F8 neighbours. The chain formation process is otherwise statistical in nature, dependent on BSP monomer concentration. The low fraction of BSP monomer units in

the reaction mixture then ensures that the copolymer will contain long sequences of F8 units, interrupted only by sparsely distributed BSP units. Further details of the F8:BSP copolymer synthesis are given in the experimental section below. We directly compare copolymer properties with the 100F8 homopolymer PFO and a blend of 90% PFO and 10% poly(9,9-dioctylfluorene-*alt*-bis-N, N'-(4-butylphenyl)-bis-N,N'-phenyl-1,4-phenylenediamine) (PFB) (with a corresponding volume fraction of 95% F8 and 5% BSP units) which we label 90PFO/10PFB. Further results are presented in the *supporting information* (SI) for the alternating 50F8:50BSP (PFB) and statistical 97F8:3BSP, 90F8:10BSP and 80F8:20BSP copolymers.

Copolymerisation of BSP and other arylamine moieties into an otherwise F8 polymer backbone reduces the ionization potential from - 5.8 eV versus vacuum for PFO to, for example, - 5.09 eV for PFB and - 4.98 eV for the corresponding alternating copolymer with methoxy substituted phenylenediamine moieties (poly(9,9-dioctylfluorene-co-bis-N,N'-(4-methoxyphenyl)-bis-N,N'-phenyl-1,4-phenylenediamine) (PFMO)).^{40–42} Varying both the arylamine moiety and its fractional incorporation within an F8-based copolymer thus provides an approach to tuning the hole injection and carrier balance properties of blue PLEDs.^{6,38,40,43,44} The associated optical gap remains large^{40,45} but because the emission acquires a more charge-transfer-like character with a broadened spectrum it is no longer suitable to address the display requirement for deep-blue luminescence despite the improvement in efficiency.

Our study looks to combine the electrical benefits of arylamine incorporation with a conformational approach to spectral control. We demonstrate deep-blue, high-efficiency and stable PLEDs by inducing the β -phase conformation within long, uninterrupted F8 chain segments of the 95F8:5BSP copolymer. This allows a significant improvement in CIE (x, y)

from (0.149, 0.175) to (0.145, 0.123) and yields peak luminous efficiency, $\eta = 3.60$ cd/A (at 146.5 cd/m²) and luminous power efficiency, $\eta_w = 2.44$ lm/W (at 10.8 cd/m²). The latter efficiency values represent state of the art performance for simple copolymer deep-blue PLEDs,^{3,4,46} being more than five-fold better than for otherwise-equivalent, glassy PFO EML PLEDs (0.70 cd/A and 0.38 lm/W) and 14 and 60 times higher, respectively, than for our first-reported PFO EML PLEDs (0.25 cd/A and 0.04 lm/W).¹⁰ Even at 1000 cd/m² the efficiencies remain high, with $\eta = 3.50$ cd/A and $\eta_w = 1.50$ lm/W.

RESULTS AND DISCUSSION

Optical absorption and photoluminescence spectroscopy. Optical absorption spectra for PFO, 95F8:5BSP copolymer and 90F8/10PFB blend films on spectrosil substrates are shown in Figures 2(a), (b), and (c), respectively, before and after solvent treatment to generate F8 β -phase chain segments. The glassy-phase spectra of the 95F8:5BSP copolymer (Figure 2 (b)) and 90F8/10PFB blend (Figure 2(c)) films closely resemble that of PFO with the main π - π^* absorption peak located at ~ 384 nm. After solvent vapor annealing (SVA) with toluene, the characteristic β -phase absorption peak at 433 nm was observed for all three samples, including the copolymer. This confirms that the BSP moieties within the copolymer backbone do not prevent β -phase chain segment formation. The small BSP fraction (5 wt%) ensures that there are sufficiently long F8 segments within which the β -phase can form; oligofluorenes with as few as five 9,9-dioctylfluorene repeat units are reported to show β -phase spectral features.⁴⁷

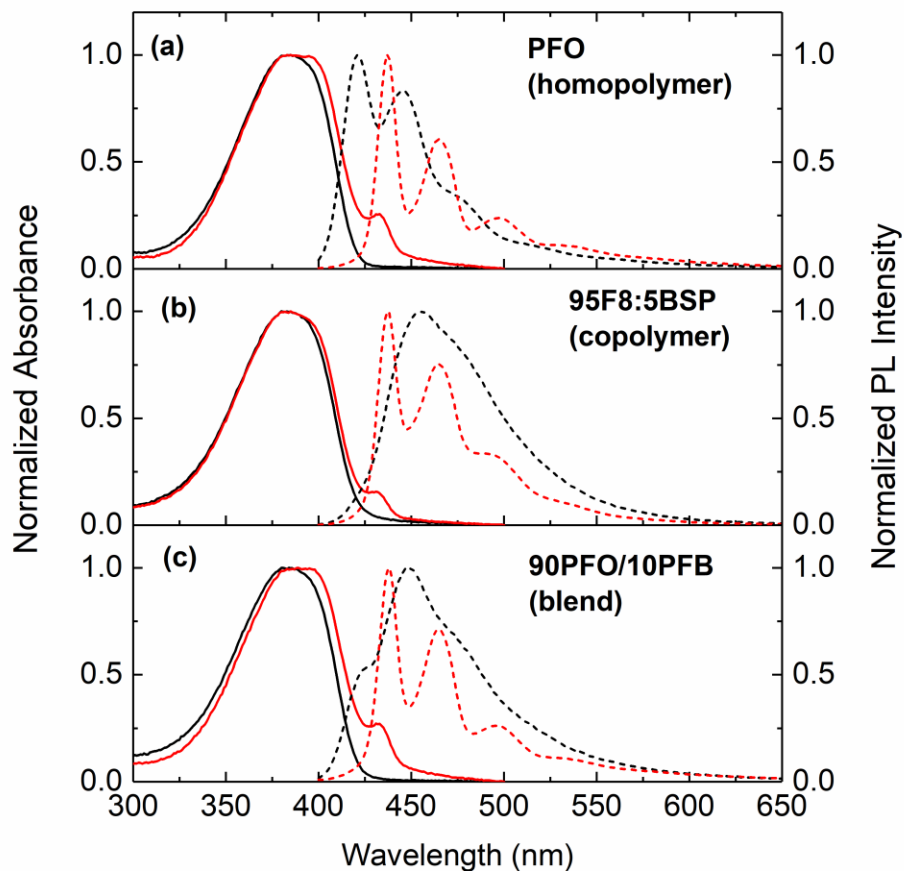


Figure 2. Peak normalized optical absorption (solid) and PL emission (dashed) spectra for (a) PFO, (b) 95F8:5BSP copolymer and (c) 90PFO/10PFB blend films spin coated on spectroil substrates. Glassy phase data are shown with black lines whilst β -phase data are shown with red lines. PL emission spectra were excited at $\lambda_{\text{ex}} = 385$ nm.

The proportion of F8 β -phase segments can be estimated by subtraction of a suitably normalized glassy phase absorption spectrum and comparison of the integrated residual (β -phase) and subtracted areas (Figure S1). Table 1 summarizes the estimated β -phase fractions for each film type.

Table 1. Estimated β -phase fractions and β -phase PL contributions in film samples of PFO, 95F8:5BSP and 90PFO/10PFB

Film type	β -phase fraction	β -phase PL contribution
PFO	$10\% \pm 2\%$	100%
95F8:5BSP copolymer	$5\% \pm 1\%$	62%
90PFO/10PFB blend	$12\% \pm 2\%$	82%

A higher fraction of β -phase chain segments is formed in films of the PFO homopolymer (10%) and 90PFO/10PFB blend (12%) than of the 95F8:5BSP copolymer (5%). The β -phase fraction in the homopolymer is broadly consistent with previous results in the literature.^{22,48} The 50F8:50BSP alternating copolymer (PFB) does not have any extended sequences of F8 units in which the β -phase can form and hence in the blend only the PFO chains support β -phase segments. We also know that bulky BSP moieties disrupt close chain packing, leading to a more disordered glassy microstructure for PFB with no observed crystallization on thermal annealing^{40,45} and no β -phase formation. It is perhaps not, therefore, surprising that the 95F8:5BSP copolymer has a smaller fraction of β -phase chain segments formed during SVA than PFO. Our study additionally shows that β -phase segment formation still occurs (to a lesser degree) for 90F8:10BSP and (marginally) 80F8:20BSP copolymer films (see Figure S2). In the case of the blend films, the 10% fraction of PFB chains (with 50% BSP content) will not support β -phase segment formation so one might expect a proportionate reduction in overall β -phase fraction relative to PFO. This is not, however, seen; most likely as a result of an increase in free volume that compensates by facilitating conformation change in the PFO chains.

The PL emission spectra for each of the three film types are shown in Figures 2(a), (b) and (c) before and after solvent treatment to generate F8 β -phase chain segments. All spectra were excited at $\lambda_{\text{ex}} = 385$ nm. The glassy homopolymer PFO film spectrum in Figure 2(a) is consistent with literature reports, with S_1 - S_0 0-0 and 0-1 vibronic peaks at 421 nm and 447 nm, respectively.^{14,24,25,27,28} The glassy 95F8:5BSP copolymer film shows a red-shifted, broad, asymmetric (with long wavelength tail), and largely featureless PL spectrum, which is very similar (but slightly red shifted (455 nm peak) and broadened) to that of the PFB component (450 nm peak) in the blend film and, indeed, the 97F8:3BSP, 90F8:10BSP and 80F8:20BSP copolymers (see Figure S2). The 95F8:5BSP copolymer film spectrum doesn't reveal an obviously PFO-like (F8-localised) component indicating efficient energy transfer from locally excited F8 excitons to BSP centered excitons.⁴⁹

The excited states responsible for the glassy copolymer PL have been shown to have significant charge transfer (CT) character⁴⁹ as observed for PFB and poly(9,9-dioctylfluorene-co-*N*-(4-butylphenyl)diphenylamine) (TFB).⁵⁰ The dilute solution PL spectra of PFO homopolymer, PFB and 95F8:5BSP for solvents of different polarity (toluene, THF and dichlorobenzene) are shown in Figure S3. The PFO PL shows little change with solvent polarity, whilst for PFB there is a large red shift and broadening with increasing polarity, strongly indicative of CT character. For 95F8:5BSP the emission comprises both vibronically-structured F8 and broadband BSP related contributions with the former experiencing no solvatochromic shift whilst the latter red-shifts and broadens, confirming a coexistence of both bound neutral exciton and CT emission states. The CT character originates from a differential spatial partitioning of the HOMO and LUMO wavefunctions across the BSP and F8 units, leading to a displacement in associated hole

and electron charge densities.⁴⁹ This is supported by cyclic voltammetry (CV) measurements (see *supporting information* Figure S4).

The PL spectra are significantly altered by the generation of β -phase chain segments. All three film-types then display well-resolved vibronic structure with a close match of the blend and copolymer PL spectral features to those of PFO; the characteristic β -phase vibronic peaks appear at 437, 465 and 498 nm. However, differences do exist, with the vibronic peaks best resolved for PFO, less so for the blend and least for the copolymer. In addition, the apparent strength of the S_1 - S_0 0-1 and 0-2 vibronic peaks relative to the 0-0 is greater for the 90PFO/10PFB blend than PFO and greatest for the 95F8:5BSP copolymer, consistent with the blend and copolymer spectra comprising a superposition of β -phase PFO-like structured excitonic emission and residual PFB-like broadband CT emission. Separation of the 95F8:5BSP copolymer and 90PFO/10PFB blend spectra in this way (Figure S5) reveals that 62% of the copolymer emission is β -phase structured emission whilst 38% is residual PFB-like emission. The 90PFO/10PFB blend shows 82% β -phase emission and 18% residual PFB emission.

Efficient energy transfer from high energy glassy to low energy β -phase segments in PFO has been extensively studied, with only a few % of β -phase segments needed for dominant β -phase emission.^{14,25,28} Intriguingly, we observe similar behavior here with the presence of β -phase segments in the copolymer and blend films leading to a strong promotion of structured vibronic emission. This is despite the fact that as a consequence there is a net increase in mean PL emission energy relative to the glassy film spectra (with dominant CT-like emission); this can be explained by the very small Stokes shift ($\lambda \sim 5$ nm) for β -phase segments. β -phase PL spectral components are also evident in the SVA 97F8:3BSP, 90F8:10BSP and 80F8:20BSP copolymer films but not for PFB (50F8:50BSP alternating copolymer) (Figure S2). As the fraction of BSP

units increases, the fraction of β -phase segments formed after SVA decreases (Table S1), resulting in larger residual fractions of PFB-like emission. Radiative decay times for the competing emissive species are likely to be important in this context.

Despite both having the same volume fraction of F8 and BSP units, the glassy phase 90PFO/10PFB blend film PL spectrum contains emission components from both PFO (evidenced by the shoulder at 425 nm) and PFB (main peak at 450 nm) polymer chains, whereas the 95F8:5BSP copolymer seemingly does not. This indicates that energy transfer from majority F8- to minority BSP-centered sites is less efficient in the blend (PFO to PFB inter-chain transfer) than found in the copolymer (for combined inter- and intra-chain transfer); blend microstructure will clearly also play a role in this.

The copolymer, in addition, shows less intense emission around 530 nm (see Figure S6(d)), where ‘green-band’ (fluorenone defect enabled) excimer emission occurs for PFO and related materials.^{12,13} A reduction in green-band emission is an advantage of incorporating bulky BSP moieties within the copolymer backbone, reducing fluorenone-to-fluorenone cofacial π -stacking, and hence excimer formation and emission.

Time dependent PL spectroscopy. To further characterize the emissive species contributing to the PL spectra, time correlated single photon counting (TCSPC) measurements were used to record PL decay transients under (unless otherwise indicated) 404 nm excitation and 460 nm detection. Figure 3 shows results for, from top to bottom, 95F8:5BSP copolymer, 90PFO/10PFB blend and PFO homopolymer thin films with both glassy (left) and β -phase (right panel) microstructures. Table 2 collects together the fitted decay times, fractional amplitudes, average decay times and photoluminescence quantum efficiencies (PLQEs). Additional decay transients collected at a range of different wavelengths between 420 and 540 nm are shown in Figure S7

and equivalent data for PFB is shown in Figure S8. PL spectra and decay transients were also measured for dilute toluene solution samples of PFO, PFB and 95F8:5PFB and are shown in Figure S9.

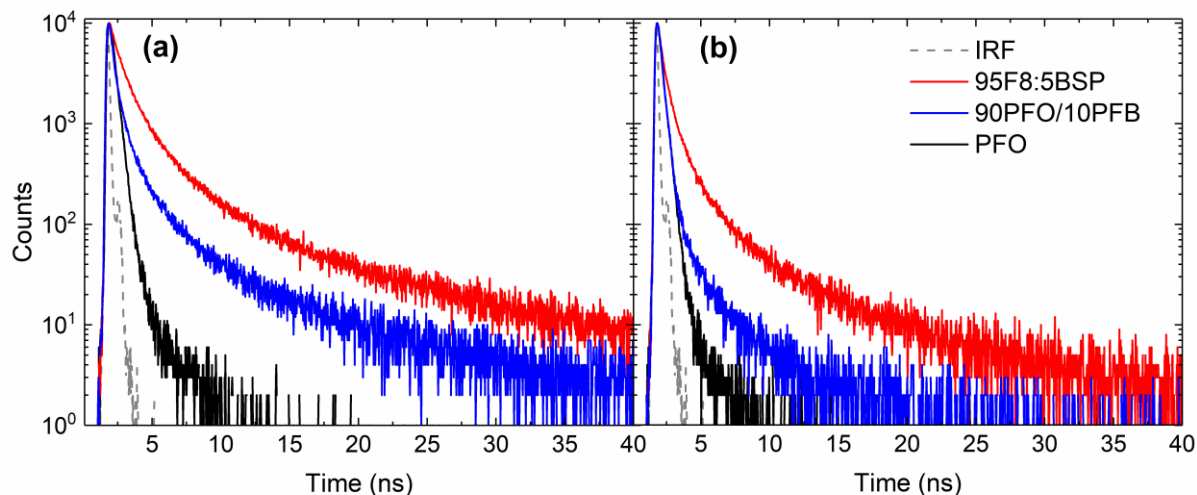


Figure 3. PL decay transients for (a) glassy- and (b) β -phase films of, from top to bottom, 95F8:5BSP copolymer (red), 90PFO/10PFB blend (blue) and PFO homopolymer (black). The measured instrument response function (IRF) is also shown (dashed grey line). Samples were excited at 404 nm and the resulting PL emission intensity was monitored at 460 nm.

Table 2. Decay times and percentage amplitudes obtained by fitting the transient PL data presented in Figure 3 to a multi-exponential decay model. The χ^2 values are indicative of the fit-quality. The average decay time is found as the weighted sum of the fitted lifetimes $\tau_{av} = \sum_i A_i \tau_i$. Photoluminescence quantum efficiency (PLQE) values are also included.

Sample	τ_1 (ns):(A ₁)	τ_2 (ns):(A ₂)	τ_3 (ns):(A ₃)	τ_{av} (ns)	χ^2	PLQE (%)
PFO Glassy	0.314:(97%)	1.34:(3%)	-	0.35	1.21	35 \pm 5
PFO β -phase	0.270:(98%)	1.15:(2%)	-	0.29	1.13	35 \pm 5

95F8:5BSP Glassy	0.580:(43%)	2.18:(45%)	11.9:(12%)	2.66	1.07	45 ± 5
95F8:5BSP β -phase	0.319:(56%)	1.32:(35%)	7.43:(9%)	1.31	0.89	40 ± 5
90PFO/10PFB Glassy	0.295:(64%)	1.48:(27)%	8.2:(9%)	1.33	0.92	20 ± 5
90PFO/10PFB β -phase	0.247:(97%)	1.93:(3%)	-	0.30	1.05	25 ± 5

The glassy PFO films yield a predominantly fast neutral singlet exciton decay with ~ 314 ps time constant, in agreement with decay times reported previously for this microstructure (~ 300 - 400 ps).^{14,27,51–53} A minor ($\sim 3\%$) fraction of longer-lived (~ 1.34 ns) PL is also observed, attributed to inter-chain/-segment states, including non-geminate pairs and fluorenone-defect-based excimers (yielding ‘green-band’ emission) (Figure S7(a)).^{13,53–55} Consistent with this assignment, the PFO decay transients for dilute solutions are mono-exponential at all detection wavelengths, with ~ 356 ps decay time (Figure S9(b)). For PFO β -phase film samples, the 460 nm decay times reduce marginally to ~ 270 ps and ~ 1.15 ns, which (given no PLQE decrease (Table 2)) points to an increase in transition dipole moment, consistent with the known increase in conjugation length.^{19,26}

The PL transients of the 95F8:5BSP copolymer in dilute solution (Figure S9(c)) show a bi-exponential decay at shorter wavelengths (420 and 440 nm), attributed to combined PFO-like excitonic emission (with $\tau_1 \sim 140$ ps) and PFB-like CT emission (with $\tau_2 \sim 1.4$ ns). At longer wavelengths, beyond 460 nm, a mono-exponential decay with $\tau \approx 1.4$ ns is observed, identical to the dilute solution decay for PFB (Figure S9(d)). In the case of glassy 95F8:5BSP copolymer films the overall decay at 460 nm can be described by three components with $\tau_1 \sim 580$ ps (43%), $\tau_2 \sim 2.18$ ns (45%) and $\tau_3 \sim 11.9$ ns (12%), each attributable to CT emission. The average lifetime

is then $\tau_{av} \sim 2.66$ ns. These time constants all differ from the solution CT-state decay, consistent with the influence of heterogeneity in solid-state packing and inter-chain/-segment interactions, as also reported in previous studies of fluorene-amine copolymers.^{49,56,57} We further note that the decay times vary substantially with emission wavelength (Figure S7(c)), again suggesting a distribution of CT lifetimes within the copolymer. Interestingly, the longest-time constant ($\tau_3 \sim 11.9$ ns) decay is not observed in PFB (50F8:50BSP alternating copolymer) (Figure S8) and its observation here then points to a potentially more substantial spatial separation of electron and hole wavefunctions in glassy 95F8:5BSP. One possibility would be inter-chain excitations formed between high electron affinity F8 units in one chain and low ionization potential BSP units in a neighboring chain. However, as no distinct exciplex peak is seen in either PL or EL this remains speculative.

The striking spectral changes that occur when β -phase chain segments are induced in 95F8:5BSP copolymer films (Figure 2(b)) are accompanied by a strong change in 460 nm PL decay dynamics (Figure 3 and Table 2). Each of the fitted decay times reduces, to $\tau_1 \sim 319$ ps (56%), $\tau_2 \sim 1.32$ ns (35%) and $\tau_3 \sim 7.43$ ns (9%), with a large shift in fractional weighting towards the τ_1 component. The average lifetime correspondingly reduces to $\tau_{av} \sim 1.31$ ns. The majority sub-320 ps decay component is consistent with the spectral dominance of vibronic F8-based emission (Figure 2(b)) whilst the 1.32 and 7.43 ns time constants signal the presence of residual CT emission. As for the glassy case, the decays are slower for longer collection wavelengths (Figure S7(d)). However, unlike the situation for PFO and blend films, a modest decrease in PLQE from 45% to 40% was observed when the β -phase was induced in copolymer films (Table 2), albeit that the PLQE itself remains relatively high (c.f. 35% for PFO and 25%

for the blend). Among possible explanations, fluorenone-centered quenching is plausible but remains unproven.

The 460 nm PL decay transient for glassy 90PFO/10PFB blend films can also be fit to three exponentials, although their relative fractions and decay times, not surprisingly, differ from those of the 95F8:5BSP copolymer (Table 2). Excitonic emission from the PFO chains is dominant, with CT-like emission accounting for much smaller fractions than in the copolymer; corresponding decay times are $\tau_1 \sim 295$ ps (64%), $\tau_2 \sim 1.48$ ns (27%) and $\tau_3 \sim 8.2$ ns (9%). As for the copolymer, when emission is collected at longer wavelengths, we see that longer lifetime emissive species are increasingly important (Figure S7(e)). In the blend case, the longest time constant excited states ($\tau_3 \sim 8.2$ ns) have previously been shown to be exciplexes generated between PFO and PFB, with thermally assisted energy transfer to a PFB CT-like exciton.⁵⁸ Upon β -phase induction, the decay becomes almost mono-exponential (Figure 3) with excitonic emission from PFO β -phase chain segments totally dominant; decay times are $\tau_1 \sim 247$ ps (97%) and $\tau_2 \sim 1.93$ ns (3%). The lack of a longer lived time constant indicates the majority excitons generated on PFO chains no longer form exciplexes with PFB and instead efficiently transfer to β -phase segments before undergoing radiative decay. As detection wavelength is increased (Figure S7(f)), the short-lived decay time remains relatively constant ($\tau \sim 271$ -325 ps) until 500 nm, where CT emission increases. The PLQE values for glassy and β -phase 90PFO/10PFB blends were 20% and 25% respectively, smaller than for both PFO and 95F8:5BSP copolymer films, indicating more substantial non-radiative decay.

Display-related Device characteristics. To test the effect of β -phase segment formation on device performance, PLEDs were fabricated (see experimental methods) with a conventional bottom-emitting device architecture, comprising glass substrate / indium tin oxide (ITO) anode /

poly(3,4-ethylenedioxythiophene) (PEDOT:PSS) hole injection layer / TFB electron blocking interlayer / emission layer (EML) / LiF / Ca / Al cathode. Schematic device and energy level diagrams are shown in Figure 4. The energy levels of PFO, 95F8:5BSP and PFB were deduced from CV measurements (Figure S4 and Table S2).

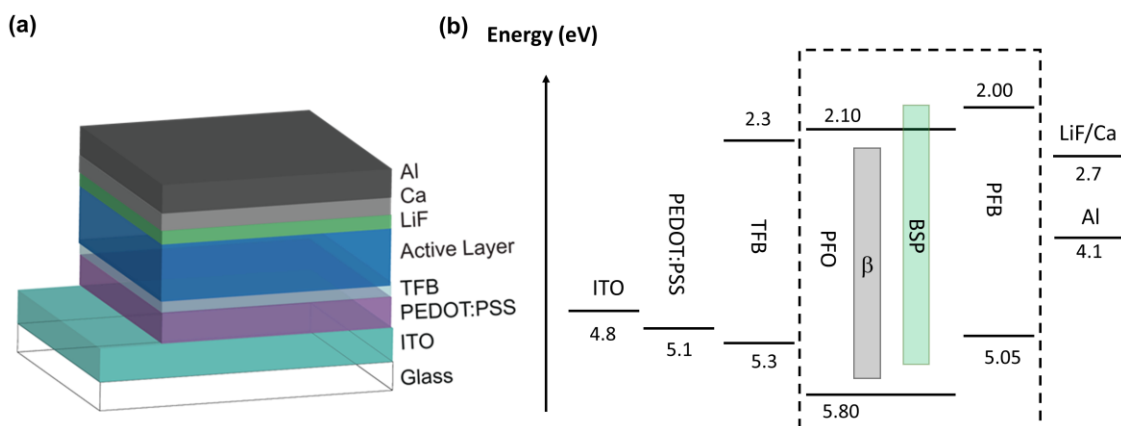


Figure 4. (a) Device structure of blue PLEDs and (b) corresponding schematic energy level diagram. The polymer energy levels were deduced from CV measurements. The shaded grey area indicates the smaller energy gap for β -phase segments in PFO and 95F8:5BSP, whilst the pale green area indicates the energy gap for BSP units within the 95F8:5BSP copolymer.

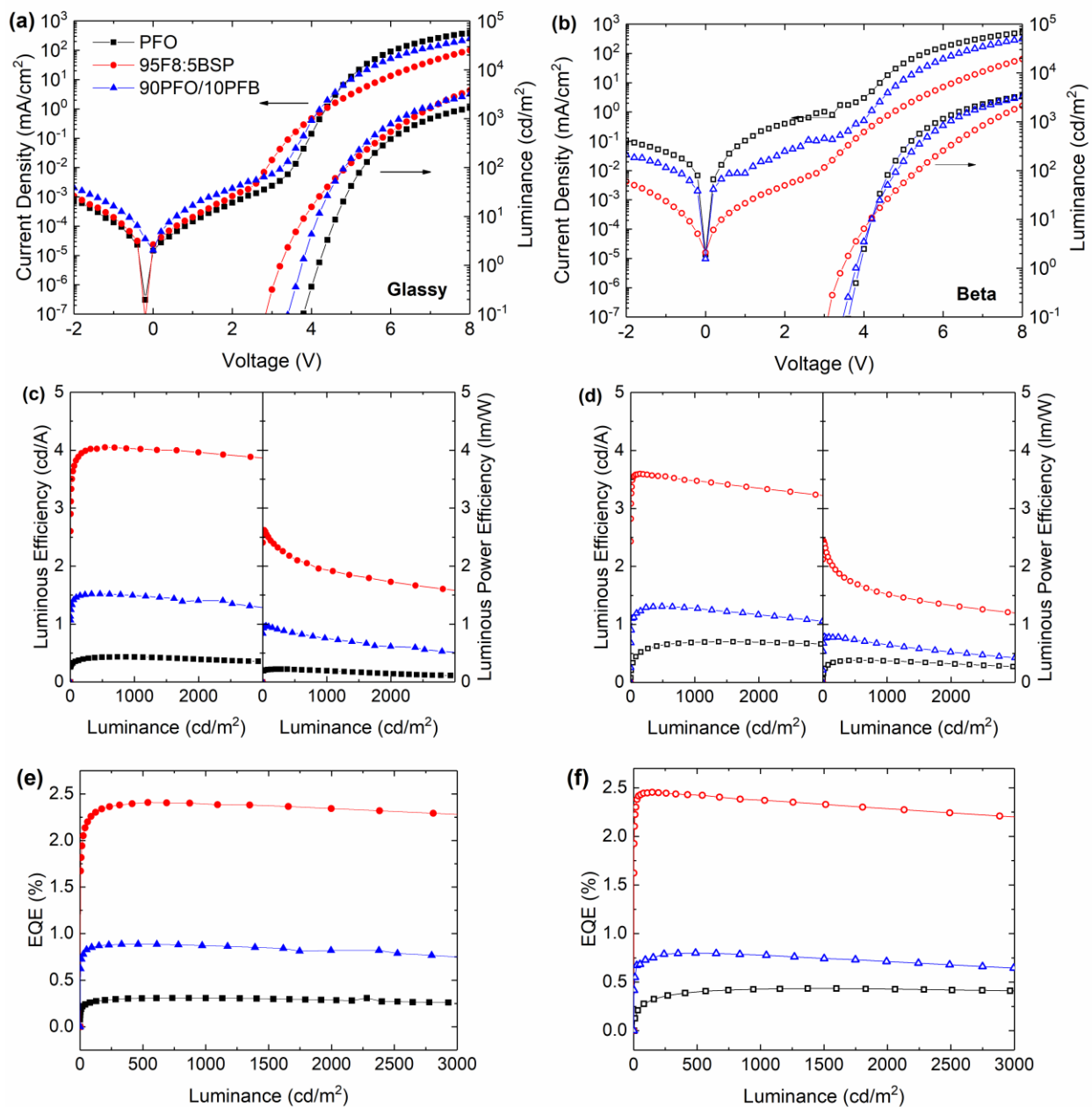


Figure 5. PLED characteristics for glassy (filled symbols, (a), (c) and (e)) and β -phase (open symbols, (b), (d) and (f)) EML film microstructure devices. J-V-L data are plotted in (a) and (b), Luminous (cd/A) and luminous power (lm/W) efficiency data as a function of luminance in (c) and (d) and associated EQE data in (e) and (f). 95F8:5BSP copolymer EML data are plotted as

red circles, 90PFO/10PFB blend data as blue triangles and PFO homopolymer data as black squares.

Figures 5 (a) and (b) compare the current density and luminance vs voltage (J-V-L) characteristics for, respectively, glassy and β -phase PFO homopolymer, 95F8:5BSP copolymer and 90PFO/10PFB blend EML devices. Figures 5 (c) and (d) show the corresponding luminance-dependent glassy and β -phase PLED efficiencies η (cd/A) and η_w (lm/W) and Figures 5 (e) and (f) the associated external quantum efficiencies η_{eqe} (EQE). Other parameters (turn-on voltage, peak η , η_w and η_{eqe}) for these devices are collated in Table 3 and their electroluminescence (EL) spectra are shown in Figure 6(a).

Table 3. Summary of best PLED performance for the current study showing turn-on voltages (defined as the voltage at which luminance reaches 1 cd/m²), peak luminous (cd/A), luminous power (lm/W) and external quantum efficiencies (%) and their values at 100 cd/m² and 1000 cd/m², and CIE (x, y) color coordinates for PFO, 95F8:5BSP copolymer and 90PFO/10PFB blend EML films with both glassy and β -phase microstructures.

EML Type	Turn-on Voltage (V)	Luminous efficiency η (cd/A)			Luminous Power efficiency η_w (lm/W)			External quantum efficiency η_{eqe} (%)			CIE (x,y)
		Peak	@ 100 cd/m^2	@ 1000 cd/m^2	Peak	@ 100 cd/m^2	@ 1000 cd/m^2	Peak	@ 100 cd/m^2	@ 1000 cd/m^2	
PFO Glassy	4.2	0.43 @ 6.8 V	0.36	0.43	0.22 @ 5.6 V	0.22	0.19	0.31 @ 6.6 V	0.26	0.31	(0.155, 0.098)
PFO β -phase	4.0	0.70 @ 6.2 V	0.48	0.69	0.38 @ 5.4 V	0.32	0.37	0.43 @ 6.0 V	0.30	0.43	(0.157, 0.117)
90PFO/10PFB Glassy	3.8	1.52 @ 5.6 V	1.47	1.48	0.97 @ 4.6 V	0.95	0.74	0.89 @ 5.6 V	0.86	0.87	(0.162, 0.174)
90PFO/10PFB β -phase	3.8	1.31 @ 5.6 V	1.21	1.28	0.79 @ 4.4 V	0.78	0.65	0.80 @ 5.6 V	0.73	0.78	(0.151, 0.118)
95F8:5BSP Glassy	3.2	4.05 @ 6.2 V	3.80	4.00	2.62 @ 4.0 V	2.50	1.90	2.40 @ 6.0 V	2.30	2.39	(0.149, 0.175)
95F8:5BSP β -phase	3.2	3.60 @ 5.6 V	3.60	3.50	2.44 @ 4.2 V	2.10	1.50	2.40 @ 5.6 V	2.44	2.37	(0.145, 0.123)

In terms of PLED efficiency, PFO glassy EML devices show a peak $\eta = 0.43$ cd/A at 6.8 V, a peak $\eta_w = 0.22$ lm/W at 5.6 V and a peak $\eta_{eqe} = 0.31\%$ at 6.6 V, with 1000 cd/m² luminance at 7 V. The PFO β -phase EML devices show a significant improvement, with peak efficiencies of $\eta = 0.70$ cd/A at 6.2 V, $\eta_w = 0.38$ lm/W at 5.4 V, $\eta_{eqe} = 0.43\%$ at 6.0 V and 1000 cd/m² luminance now at 5.9 V. This improvement is consistent with previous reports for β -phase PFO devices.^{30,31,33,59,60} Figure 6(b) shows, however, that the efficiency gains are at the expense of a detrimental change in EL emission color; a consequence not previously emphasized. The shift from glassy (peak $\lambda = 425$ nm) to β -phase (peak $\lambda = 440$ nm) alters the CIE (x, y) coordinates from (0.155, 0.098) to (0.157, 0.117), with a corresponding shift in dominant wavelength from 470 to 475 nm and a decrease in color saturation from 86 to 82%. This behavior limits the achievable display color gamut. It also helps to explain why the η_{eqe} enhancement is more modest than the gains in η and η_w ; a shift to the green leads to a better overlap with the photopic eye sensitivity function that peaks at 555nm.

The 90PFO/10PFB blend EML PLEDs show significantly better efficiency characteristics than for the corresponding PFO devices (Figure 5), with the PFB fraction strongly assisting hole injection (Figure 4(b)).^{40,45} The glassy blend EML gives peak efficiencies $\eta = 1.52$ cd/A at 5.6 V, $\eta_w = 0.97$ lm/W at 4.6 V and $\eta_{eqe} = 0.89\%$ at 5.6 V, with a luminance of 1000 cd/m² at 6.3 V, whilst β -phase blend EML devices show peak efficiencies $\eta = 1.31$ cd/A at 5.6 V, $\eta_w = 0.79$ lm/W at 4.4 V and $\eta_{eqe} = 0.80\%$ at 5.6 V and reach 1000 cd/m² at 6.2 V. β -phase devices are, therefore, somewhat less efficient than glassy devices but in terms of CIE (x, y) color coordinates β -phase segment formation leads to a shift from (0.162, 0.174) to (0.151, 0.118), resulting in a highly desirable, deeper-blue emission (Figure 6(b)). The corresponding dominant wavelength shifts from 478 to 474 nm and color saturation increases from 73 to 83%. This color

shift also helps to explain at least in part the proportionately larger decrease in η and η_w values than in η_{eqe} as the emission then has reduced overlap with the photopic eye sensitivity function.

Glassy and β -phase 95F8:5BSP copolymer EML devices show yet further enhanced PLED efficiency (Table 3). Glassy devices give peak efficiencies $\eta = 4.05$ cd/A at 6.2 V, $\eta_w = 2.62$ lm/W at 4.0 V and $\eta_{eqe} = 2.40\%$ at 6.0 V, with a luminance of 1000 cd/m² at 6.6 V, whilst for β -phase devices $\eta = 3.60$ cd/A at 5.4 V, $\eta_w = 2.44$ lm/W at 4.2 V and $\eta_{eqe} = 2.40\%$ at 5.6 V, with 1000 cd/m² at 7.2 V. Interestingly, here η_{eqe} is unaltered by β -phase induction whilst (see Figure 6(b)) the CIE (x, y) coordinates still shift positively from (0.149, 0.175) to (0.145, 0.123), resulting in a dominant wavelength decrease from 479 nm to 474 nm and a color saturation increase from 77% to 85%. Figure S10 shows the deconvolution of the EL spectra of β -phase copolymer and blend devices, showing β -phase emission accounts for $\sim 67\%$ of the total EL emission in the copolymer device, and $\sim 80\%$ emission in the blend device.

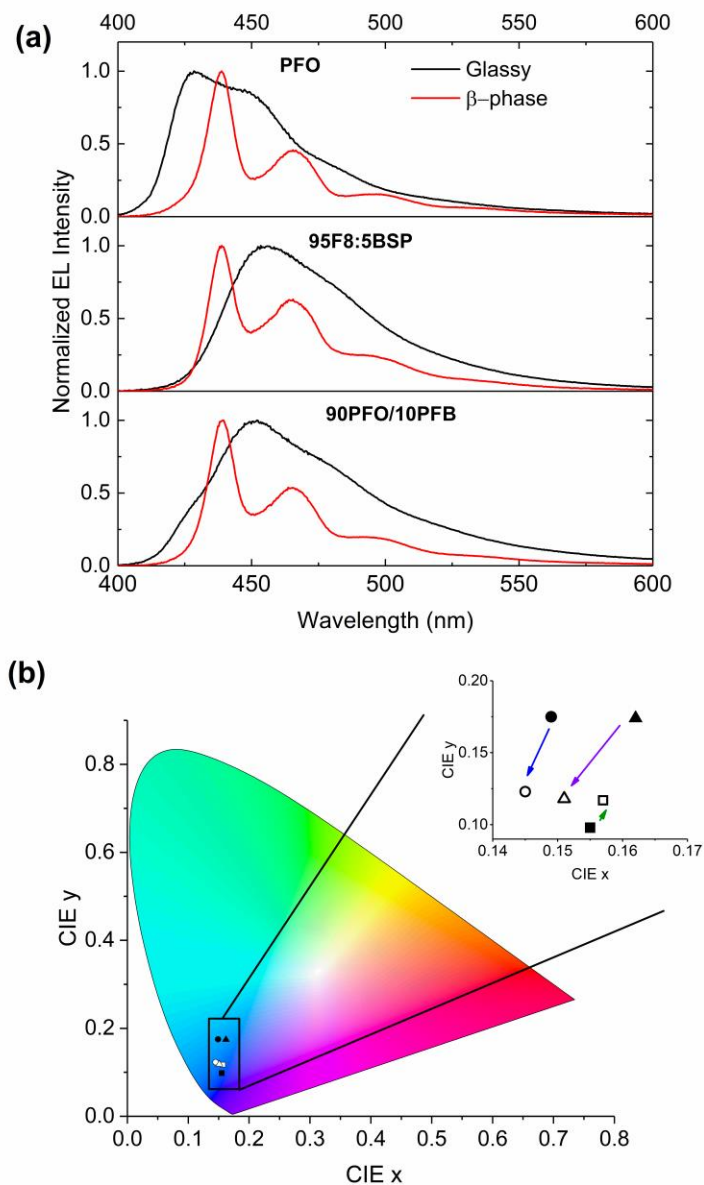


Figure 6. (a) EL spectra at 6 V for PFO homopolymer, 95F8:5BSP copolymer and 90PFO/10PFB blend devices with glassy (black) and β -phase (red) EML microstructures. (b) Color coordinate (CIE(x,y)) diagram showing the EL emission coordinates for PFO (square), 95F8:5BSP (circle) and 90PFO/10PFB (triangle) for glassy (filled black symbols) and β -phase (filled white symbols) EMLs. Inset shows EL emission coordinates on expanded scale; arrows

indicate color shift from glassy to β -phase for PFO (green arrow), 95F8:5BSP copolymer (blue arrow) and 90PFO/10PFB blend (purple arrow).

The copolymer EML efficiency improvement is largely attributed to the BSP units both assisting hole injection and, due to their sparse distribution, acting as deep hole-traps. Glassy PFO EML devices display the highest turn-on voltages (defined as the applied bias at which $L = 1 \text{ cd/m}^2$), namely 4.2 V, reducing to 4.0 V on induction of β -phase chain segments, consistent with previous reports.^{30,31,59} The 90PFO/10PFB blend devices conversely show the same turn-on voltage (3.8 V) irrespective of glassy or β -phase microstructure, as also do the 95F8:5BSP copolymer devices (3.2 V); injection is clearly controlled by BSP rather than β -phase units. The better turn-on behavior for the copolymer devices is likely due to the more uniform distribution of BSP units; they are present within every 95F8:5BSP polymer chain. Atomic force microscopy (AFM) topography images show evidence of phase segregation between PFO and PFB chains in 90PFO/10PFB blend samples (Figure S11) along with an increase in roughness (Table S3) whilst the 95F8:5BSP microstructure appears featureless. Evidence of phase segregation between PFO and PFB chains has also been previously observed in literature.⁵⁸

Other studies have additionally shown that such copolymers have three to four orders of magnitude lower time-of-flight photocurrent hole mobility (μ_h^{ToF}) than equivalent films of PFO and *alternating* fluorene-arylamine copolymers.^{40,43,45} The measured $\mu_h^{\text{ToF}} \approx 10^{-7} \text{ cm}^2/\text{Vs}$ for glassy films indicates substantially deeper hole trapping than for β -phase segment formation in PFO. Electrochemical data (Figure S4 and Table S2) for 95F8:5BSP films suggest that the trap depth is $\sim 0.3 \text{ eV}$ above the $\sim 5.80 \text{ eV}$ HOMO level of PFO. This trapping effect is also evident in the reduction in current density between the PFO homopolymer and 95F8:5BSP copolymer EML devices. We find $J = 231.4 \text{ mA/cm}^2$ at 7 V for glassy PFO, and only 41.4 mA/cm^2 at the

same voltage for glassy 95F8:5BSP despite the turn-on voltage for the copolymer (3.2 V) being 1 V lower than for PFO (4.2 V).

A well-known drawback to using PFO as the EML in PLEDs is its low spectral stability under operation due to the appearance of a low energy ‘green-band’ emission when driven at higher voltages, the origin of which is inter-chain emission from fluorenone-based defects.^{13,54,59,61} Figure 7 shows EL spectra as a function of applied voltage for glassy and β -phase PFO and 95F8:5BSP devices. As the voltage is driven beyond 7 V for the glassy PFO device and beyond 9 V for the β -phase PFO device, the emergence of a broad, low energy component (‘green-band’) is clearly observed. However for both glassy and β -phase 95F8:5BSP devices, no green-band is observed when driving devices between 5 and 13 V, indicating that 95F8:5BSP devices show much improved color stability compared with PFO PLED devices. This is likely to be due to the bulky BSP units causing increased disruption in the packing structure between the polymer chains, thereby preventing green band emission; similar reductions in green band have been observed when small amounts of carbazole units or large amine group end caps have been incorporated into polyfluorene chains.^{62,63}

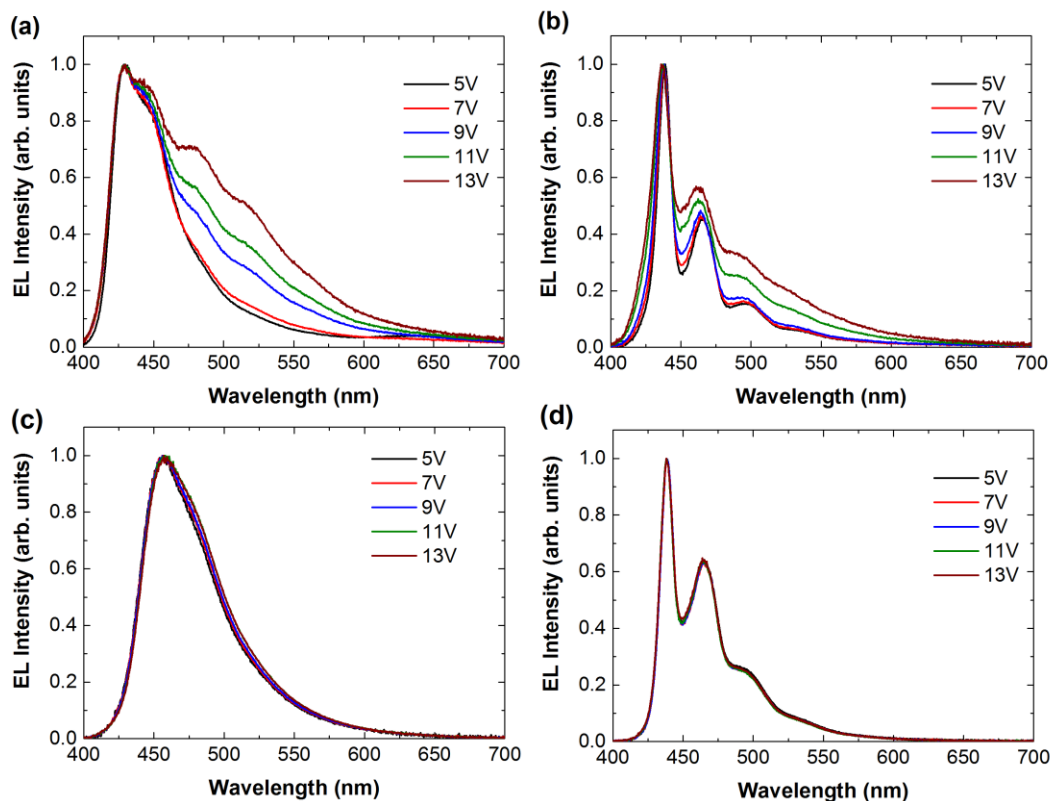


Figure 7. EL spectra as a function of voltage for (a) glassy phase PFO, (b) β -phase PFO, (c) glassy phase 95F8:5BSP and (d) β -phase 95F8:5BSP PLED devices

The BSP-centered hole trapping increases the likelihood of exciton formation and improves charge carrier balance.^{6,64} Copolymer devices based on 97F8:3BSP and 90F8:10BSP EMLs were also fabricated (Figures S12 and S13), revealing that the 95F8:5BSP copolymer gives the optimal EML efficiency performance in this composition sequence (Table S4); one needs enough but not too much BSP incorporation and the way in which the BSP units are incorporated also matters.

In summary, the device efficiency and display color parameter data (Table 4) show that in the absence of BSP units (PFO homopolymer) the induction of β -phase chain segments is advantageous to device efficiency but only at the expense of a shift away from desirable deep

blue emission. The introduction of BSP units into the EML (blend and copolymer) yields a significant overall enhancement in device efficiency and color stability with the copolymer performing substantially better than the blend. Again, though, the efficiency enhancement is achieved at the expense of color response with the BSP-related CT-like emission yielding less deep-blue color coordinates (green shift in dominant wavelength and reduction in saturation). Induction of β -phase chain segments is then strongly beneficial to the color response and for copolymer EML devices this occurs without any appreciable decrease in quantum efficiency; the β -phase copolymer EML PLEDs thus provide the best overall combination of efficiency and color performance.

Table 4. Display color parameters for PFO, 90PFO/10PFB blend and 95F8:5BSP copolymer EML PLEDs. Note the close agreement for β -phase EML color saturation and dominant wavelength for all three EML types and likewise the close agreement for glassy EML copolymer and blend devices.

EML Type	EQE (%) @ 1000 cd/m²	CIE (x,y)	Dominant Wavelength (nm)	Color Saturation (%)
PFO Glassy	0.31	0.155, 0.098	470	86
PFO β -phase	0.43	0.157, 0.117	475	82
90PFO/10PFB Glassy	0.87	0.162, 0.174	478	73
90PFO/10PFB β -phase	0.78	0.151, 0.118	474	83
95F8:5BSP Glassy	2.39	0.149, 0.175	479	77
95F8:5BSP β -	2.37	0.145, 0.123	474	85

phase				
-------	--	--	--	--

As a final device test, motivated by literature reports that β -phase formation in PFO increases device lifetime,⁵⁴ encapsulated pre- and post-SVA 95F8:5BSP copolymer PLEDs were subjected to accelerated lifetime testing under nitrogen using a constant current source set to deliver 4 mA (i.e. $J \approx 90 \text{ mA/cm}^2$ for the 4.5 mm^2 pixels under test). The luminance was measured at 60-second intervals starting from 2821 cd/m^2 for glassy and 2300 cd/m^2 for β -phase devices. Initially (c.f. Figure S14), the glassy and β -phase 95F8:5BSP PLED luminance values decayed at a similar rate, with half decay times $T_{50\%}$ (glassy) = 176 mins and $T_{50\%}$ (β -phase) = 180 mins. The subsequent decay was much more rapid in the glassy copolymer EML devices, especially beyond 400 mins. The luminance took 490 mins to drop to 30% of its starting value for the glassy 95F8:5BSP PLED, but took 630 mins to reach the same fractional output for the β -phase device, and whilst the latter was still emitting some 250 cd/m^2 at 1200 mins the glassy device luminance had fallen below 4 cd/m^2 by that time. The operational stability of β -phase 95F8:5BSP copolymer devices is, therefore, significantly greater than that of otherwise equivalent glassy devices. Several factors are expected to contribute to this including a desirable distribution of the recombination sites vertically through the EML, enhanced charge carrier balance and a faster radiative decay time for the exciton.

We now consider further the effects of β -phase formation on the energy transfer of emissive species in order to explain the desirable PLED emission for 95F8:5BSP copolymer EML devices. We explore, in particular, the origin of efficient energy transfer to β -phase F8-centred excitons, with concomitant net increase in mean photon energy and deeper-blue emission.

The HOMO and LUMO of glassy phase PFO homopolymer films were deduced from CV measurements to be 5.80 eV and 2.10 eV respectively (Figure S4 and Table S2), similar to previously reported values.⁴² Upon β -phase chain segment formation a smaller optical gap component is introduced into the ensemble of absorbing chromophores, with the resolved S_0 - S_1 0-0 peak at 433 nm.^{24,27} Additionally, as a result of rapid energy migration to β -phase segments, there is a ~ 16 nm red-shift in S_1 - S_0 0-0 PL emission. CV-measurement-based HOMO and LUMO values were also determined for PFB and 95F8:5BSP, yielding 5.05 eV and 2.00 eV and 5.49 eV and 2.10 eV, respectively (Table S2).

The schematic energy level diagram for glassy 95F8:5BSP copolymer chains (Figure 8(a)) shows how the energy levels vary spatially along the copolymer chain, with the electron-rich BSP unit being raised in energy relative to the F8 units. Whilst electrical excitation should (at least initially) predominantly produce CT excitons due to the strong hole trapping nature of the BSP units,^{6,38,43} under optical excitation exciton states will also form on longer F8 segments (labelled I in Figure 8). In this case, efficient inter- (not shown) and intra-chain energy transfer of F8 excitons to CT states (labelled II in Figure 8) is observed.⁴⁹

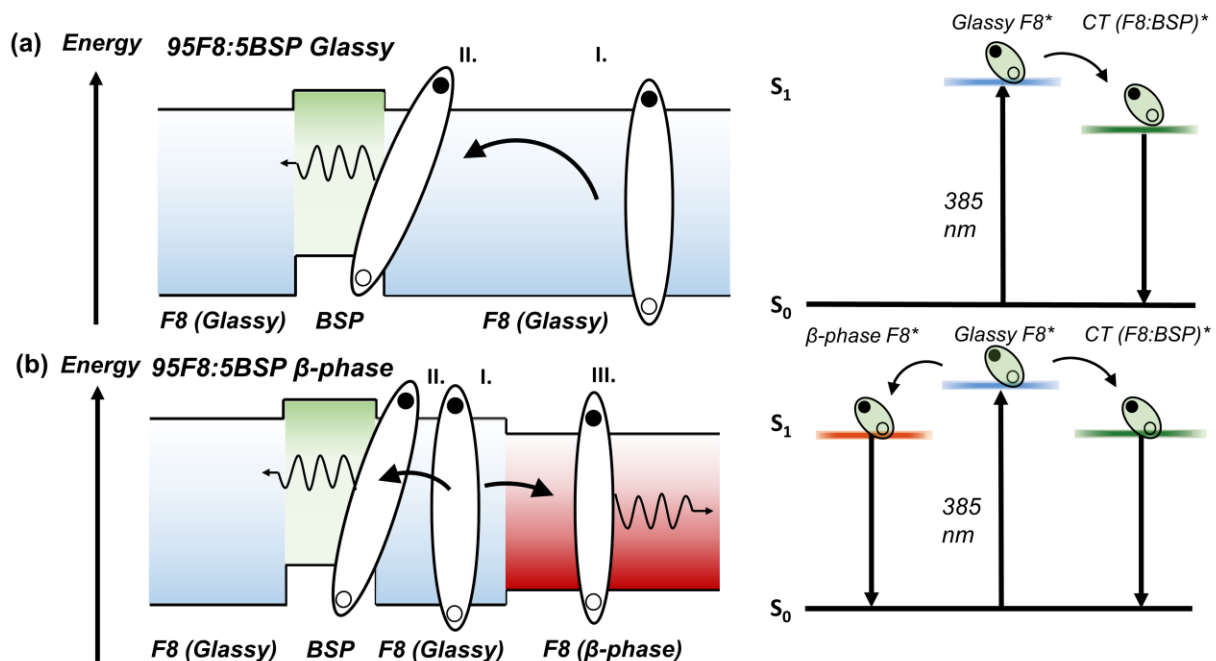


Figure 8. Schematic energy level diagrams (left column) for intra-chain energy transfer processes in 95F8:5BSP (a) glassy- and (b) β -phase chains following optical excitation. Jablonski diagrams for each process are shown to the right of each schematic. See text for explanation of numbering I, II, and III.

Upon β -phase formation, the corresponding F8 HOMO level will move up and the LUMO down, forming a Type I quantum-well-like structure along the polymer chain (Figure 8(b)).⁶⁵ Under optical excitation, excitons formed locally on glassy F8 segments undergo efficient energy transfer to either a β -phase F8 segment^{15,27,52} (labelled III in Figure 8) or BSP-based CT states⁴⁹ before decaying (Figure 8(b)). As such, the 95F8:5BSP β -phase PL spectrum is a superposition of both PFO-like β -phase emission ($\sim 62\%$ of total emission) and residual CT emission ($\sim 38\%$). The reason β -phase emission dominates the spectrum despite the film having roughly the same proportion of β -phase segments and BSP units ($\sim 5\%$) is likely to be a result of the faster decay for β -phase F8 excitons. Longer-lived CT states will be more prone to thermal energy transfer

before decay. Nevertheless, as expected, the fraction of CT type emission increases (and β -phase emission correspondingly decreases) as more BSP units are incorporated into the copolymer chain (see Figure S2 for 90F8:10BSP and 80F8:20BSP UV-vis absorption and PL emission data).

To further probe the energy transfer mechanism in the 95F8:5BSP copolymer, additional low temperature PL measurements ($\lambda_{\text{ex}} = 400$ nm) were taken for β -phase PFO and both glassy and β -phase 95F8:5BSP copolymer samples (Figure S15) from 290K down to 10 K. Low temperature β -phase 95F8:5BSP PL measurements (Figure S15(c) and (d)) reveal that the spectrum remains a superposition of both vibronic β -phase emission (Figure S15(a)) and CT-like emission from BSP centered states (Figure S15(b)) over the whole 10 to 290 K range. Spectral deconvolution reveals that the component spectra are identical to the PFO β -phase and glassy 95F8:5BSP spectra at each temperature, as for example shown at 10 K Figure S15(e). By integrating the component spectra at each temperature we find that (Figure S15(f)) the fraction of β -phase emission decreases as temperature decreases, from ~64% at 290 K to ~32% at 10 K.

These results support the energy transfer model outlined above since energy transfer in β -phase PFO has been proposed to be a two-step process of thermally assisted exciton diffusion followed by Forster resonance energy transfer from high energy glassy phase F8 to low energy β -phase segments.²⁴ The decrease in β -phase emission at low temperature could then be explained as a result of energy transfer to β -phase units being more dependent on thermally assisted diffusion than is the case for BSP sites. Alternatively, enhanced polaron formation has been previously observed for β -phase PFO and polarons are known to act as emission quenching sites, especially at low temperatures where their lifetimes are long, leading to an increasing β -

phase exciton quenching at low temperatures.²⁴ Similar effects are seen in other polymers when segmentation by conjugation breaks leads to polaron trapping.⁶⁶

Under electrical excitation of copolymer EML devices, it is likely that a much greater fraction of initially formed excitations are CT states, due to the hole trapping nature of the BSP unit (trap depth ~ 0.3 eV). Despite this, F8 β -phase emission provides the dominant ($\sim 67\%$) contribution to the EL spectrum, with residual CT-like emission delivering a more modest ($\sim 33\%$) contribution. This suggests that either endothermic energy transfer from BSP-centered CT states to β -phase F8 excitons or ‘trap-filling’ of BSP sites occurs. In the latter case, as the BSP ‘traps’ fill, β -phase F8 charge localization is expected to play an increasing role. Evidence for this is clearly seen in Figure S16, where the relative fraction of β -phase exciton EL emission increases with voltage. The shorter emission decay time for F8 β -phase segment- than BSP-localized states also feeds into the higher relative fraction of β -phase EL.

A key difference for 90PFO/10PFB blend samples is that inter-molecular energy transfer between neighboring PFB and PFO chains becomes important. Under optical excitation of the glassy-phase blend, excited states are formed directly on both PFO and PFB chains. However, due to the raised HOMO and LUMO energies of PFB relative to PFO, a type II heterojunction occurs at the PFO/PFB interfaces, resulting in exciplex formation.⁵⁸ At room temperature, the exciplex undergoes endothermic energy transfer to the emissive PFB CT state yielding its characteristic spectrum (Figure S17).⁵⁸ However, not all the PFO excitons generated will form an exciplex and we consequently also observe PFO exciton emission as a shoulder at 425 nm (Figure 2(c)). Under electrical excitation, as holes will tend to localize on PFB chains and electrons on PFO (see Figure 4 energy levels) it is likely that exciplexes are directly formed by electron-hole Coulomb capture⁶⁷ before undergoing endothermic energy transfer to PFB CT

states (Figure S18). Consistent with this, Figure 6(a) indeed shows a much weaker 425 nm PFO emission shoulder for glassy phase blend EL than PL.

For β -phase blends, the majority of optically excited glassy segment F8 excitons will tend to transfer their energy to β -phase sites without forming exciplexes (Figure S17). Additionally, under electrical excitation, exciplex states that form between PFB and β -phase PFO chains (from direct electron-hole capture) will likely undergo endothermic energy transfer to PFO β -phase excitons (Figure S18). As a consequence, both the PL (Figure 2(c)) and EL (Figure 6(a)) β -phase spectra are dominated by structured vibronic emission. Some residual CT emission remains, respectively 18% and 20% for PL and EL (Figures S5 and S10), but these values are significantly lower than for the 95F8:5BSP copolymer case despite the same volume fraction of BSP units being present. This is most likely due to the greater fraction of β -phase segments generated and the consequences of phase separation.

CONCLUSION

In summary, we have demonstrated a novel route to high-efficiency, deep-blue emitting PLEDs by introducing a simple molecular-level conformation change in the F8 sequences of 95F8:5BSP copolymers from the disordered glassy phase to the rigid β -phase microstructure *via* annealing in a toluene solvent atmosphere. UV-visible absorption and PL spectroscopy measurements of solvent annealed F8:BSP copolymers at 3%, 5%, 10% and 20% BSP fraction showed β -phase formation in the F8 segments, with the appearance of characteristic red-shifted absorption peaks and the promotion of well-structured vibronic emission.

Incorporating 5% BSP units into the conjugated backbone of an otherwise F8 polymer (thus yielding 95F8:5BSP) produces a five-fold performance enhancement in PLED luminous

efficiency and luminous power efficiency relative to PFO (i.e. 100F8). The BSP units (with significantly lower ionization potential) enhance hole injection and act as hole-trapping sites that assist efficient exciton formation. The BSP units have an additional benefit in increasing the color stability of the PLEDs by suppressing green-band emission when driven at higher voltages. The BSP units also, however, undesirably shift the EL to a CT-state-based sky-blue emission spectrum (CIE (x, y) = (0.149, 0.175)). Subsequent introduction of β -phase chain segments within the copolymer restores a more desirable deep-blue, vibronically-structured EL emission with CIE (x, y) = (0.145, 0.123) whilst retaining the bulk of the efficiency enhancement; it also increases operational stability. The overall best PLEDs, using β -phase 95F8:5BSP EMLs, then have $\eta = 3.60$ cd/A at 5.4 V and $\eta_w = 2.44$ lm/W at 4.2 V, with 1000 cd/m² luminance at 7.2 V.

The spatial distribution of BSP units in the PLED active layer is also found to be significant to device function, with 95F8:5BSP copolymer (homogeneous) and 90PFO/10PFB blend (heterogeneous) EMLs showing distinct properties despite containing the same volume fraction of BSP units. Both the glassy- and β -phase 90PFO/10PFB blend devices performed less well than equivalent copolymer devices with luminous efficiency, luminous power efficiency and EQE lower by a factor 2.5-3.0 but still significantly better than for PFO-only EML devices.

Our study represents the first demonstration of the use of a simple molecular-level chain conformation change as a vector to control the optoelectronic properties of a fluorene-based copolymer. It will be interesting to see how broadly our conformation control approach can be applied to materials systems for other device applications, including solar energy conversion, electronics and sensing.

EXPERIMENTAL

Materials. PFO, 95F8:5BSP and 50F8:50BSP were supplied by Cambridge Display Technology Ltd and used as received. The weight-average molecular weights (M_w) and polydispersity indices (PDIs) were 1.04×10^5 g/mol and 2.3 for PFO, 2.77×10^5 g/mol and 2.4 for 95F8:5BSP and 1.32×10^6 g/mol and 2.0 for PFB (50F8:50BSP). Additional samples of 97F8:3BSP, 95F8:5BSP, 90F8:10BSP, 80F8:20BSP and 50F8:50BSP copolymers were provided by the Sumitomo Chemical Company Tsukuba Research Laboratory and again used as received. All (100-x)F8:xBSP polymers were synthesized via Suzuki coupling, with the fraction x controlled by the monomer composition of the reaction mixture. This comprised 50% boronic ester disubstituted F8, (50-x)% bromine disubstituted F8 and x% bromine disubstituted BSP. The coupling process links carbon atoms with a boronic ester substituent to carbon atoms with a bromine substituent and thus creates F8-F8 and F8-BSP linkages but not BSP-BSP linkages.

UV-Vis absorption, photoluminescence spectroscopy and transient photoluminescence decay measurements. Optical spectroscopy was undertaken on ~60 nm thickness PFO homopolymer, F8:BSP copolymer and polymer/polymer blend films spin-coated from toluene solution (10 mg/ml) onto quartz substrates. The substrates had been pre-cleaned by sequential 15 minute sonications in acetone, isopropanol, and detergent (Hellmanex III, 2% by volume in DI water) prior to a 3 minute plasma ash in air at 80 watts.

Steady state transmittance was measured using a Shimadzu UV-2550 UV-visible spectrophotometer. Absorbance was calculated directly from transmittance (no scattering or reflection correction) based on the natural logarithm and the substrate contribution simply subtracted. Photoluminescence spectra were recorded in reflection geometry using a Jobin Yvon Horiba Fluoromax-3 spectrofluorometer (excitation wavelength $\lambda_{ex} = 385$ nm). PLQE was

measured using a Jobin Yvon Horiba Fluoromax-3 spectrofluorometer equipped with a diffusely reflecting integrating sphere.

Time-resolved photoluminescence decay measurements used an IBH fluorescence lifetime spectrometer operating in time-correlated single photon counting (TSPC) mode. The excitation source was a 404 nm pulsed LED operating at 1 MHz rep-rate with a pulse temporal width of 200 ps. IBH Datamax software was used to deconvolve the instrument response function from the data and to fit multi-exponential decay functions.

Low temperature photoluminescence measurements. Samples were held inside a helium filled, closed-cycle cryostat, with spectra recorded at 20 K intervals. The cryostat temperature was held constant for 5 minutes prior to each measurement, enabling the sample to reach thermal equilibrium. Excitation (0.13 mW) was with 400 nm light from a monochromated supercontinuum laser source (Fianium). PL was collected at right angles to excitation using a 100 μm diameter optical fibre and fed into a spectrometer (Andor SR-163) equipped with a CCD detector (Andor i-Dus). To enhance the signal to noise ratio more than one hundred 0.1 s duration measurements were averaged. A dark background was subtracted from all spectra before correcting with a calibration file measured for a standard light source that accounts for the detector spectral response. The optical geometry of the experiment was unaltered between sequential temperature measurements.

PLED fabrication and characterization: The PLED device architecture consists of a multilayer stack comprising ITO/PEDOT:PSS/TFB/EML/LiF/Ca/Al. ITO anode structures on glass substrates (size 12 mm x 8 mm) were cleaned for 15 minutes each in a sequence of ultrasonic baths using acetone, isopropanol and detergent (Hellmanex III, 2% by volume in DI water). This was followed by oxygen plasma ashing in an Emitech K1050X. Next, a 35nm

thickness film of PEDOT:PSS (Clevios P VP) was deposited as hole injecting layer by spin-coating at 3000 rpm and annealing in air for 15min at 135 °C. This was followed by spin-coating (at 1000 rpm) a 15 nm thickness electron-blocking TFB interlayer from 2 mg/ml toluene solution, and then baking in nitrogen at 180 °C for one hour. The 95F8:5BSP EML (60 nm thickness) was deposited on top of the TFB interlayer, again by spin coating, at 2500 rpm from a 10 mg/ml toluene solution. For the 90PFO/10PFB blend EML, PFO and PFB toluene solutions were separately prepared and mixed to give the desired weight ratio before spin-coating (2500 rpm) to a thickness of 60 nm. Finally for PFO EML samples, toluene solutions were spin-coated (2500 rpm) to a thickness of 60 nm. To induce β -phase chain segments in the EMLs, each sample was solvent vapor annealed in a toluene atmosphere at 50 °C for 2 hours. An MBraun thermal evaporator was used to deposit the top cathode comprising a triple layer of LiF (2 nm), calcium (30 nm) and aluminum (100 nm).

PLEDs were characterized at room temperature in a sealed sample chamber under nitrogen, using a computer-controlled Keithley Source Measure unit to apply a bias voltage to the chosen pixel (each substrate accommodated 6 PLED pixels) and to measure the resultant current. A Minolta LS100 spot luminance meter measured the corresponding pixel luminance and electroluminescence spectra were recorded using an Ocean Optics USB 2000 CCD spectrometer equipped with a fiber light collection bundle. Accelerated lifetime testing was performed using the same experimental apparatus.

ASSOCIATED CONTENT

Supporting Information. The supporting information (PDF) contains: UV-vis absorption and photoluminescence measurements for 97F8:3BSP, 90F8:10BSP, 80F8:20BSP and PFB;

additional TCSPC measurements in solution and thin film; deconvolution of UV-vis and PL measurements; characterization of 97F8:3BSP and 90F8:10BSP PLEDs; and additional energy transfer diagrams for 90PFO/10PFB blends.

AUTHOR INFORMATION

Corresponding Authors

*Email: ji-seon.kim@imperial.ac.uk

*Email: donal.bradley@mpls.ox.ac.uk

Notes

The authors declare no competing financial interest.

ACKNOWLEDGMENT

IH, NC, NJC and MD acknowledge the provision of UK Engineering and Physical Sciences Research Council (EPSRC) Plastic Electronics Doctoral Training Centre (EP/G037515/1) and Cambridge Display Technology Ltd (CDT) EPSRC CASE studentships. The authors would also like to acknowledge additional research funding from CDT, the University of Oxford and EPSRC (EP/G037515/1) and thank CDT for supplying PFO, 95F8:5BSP and PFB polymers and Dr Toshihiro Ohnishi of the Sumitomo Chemical Company Tsukuba Research Laboratory for supplying 97F8:3BSP, 95F8:5BSP, 90F8:10BSP and 80F8:20BSP copolymers. We further thank Alexander Giovannitti for help with GPC and CV measurements.

REFERENCES

- (1) Burroughes, J. H.; Bradley, D. D. C.; Brown, A. R.; Marks, R. N.; Mackay, K.; Friend, R. H.; Burns, P. L.; Holmes, A. B. Light-Emitting Diodes Based on Conjugated Polymers. *Nature* **1990**, *347*, 539–541.
- (2) Lee, S. J.; Park, J. S.; Yoon, K. J.; Kim, Y. I.; Jin, S. H.; Kang, S. K.; Gal, Y. S.; Kang, S.; Lee, J. Y.; Kang, J. W.; et al. High-Efficiency Deep-Blue Light-Emitting Diodes Based on Phenylquinoline/carbazole-Based Compounds. *Adv. Funct. Mater.* **2008**, *18* (24), 3922–3930.
- (3) Cook, J. H.; Santos, J.; Li, H.; Al-Attar, H. A.; Bryce, M. R.; Monkman, A. P. Efficient Deep Blue Fluorescent Polymer Light-Emitting Diodes (PLEDs). *J. Mater. Chem. C* **2014**, *2* (28), 5587–5592.
- (4) Trattnig, R.; Pevzner, L.; Jäger, M.; Schlesinger, R.; Nardi, M. V.; Ligorio, G.; Christodoulou, C.; Koch, N.; Baumgarten, M.; Müllen, K.; et al. Bright Blue Solution Processed Triple-Layer Polymer Light-Emitting Diodes Realized by Thermal Layer Stabilization and Orthogonal Solvents. *Adv. Funct. Mater.* **2013**, *23* (39), 4897–4905.
- (5) Zhang, T.; Wang, R.; Ren, H.; Chen, Z.; Li, J. Deep Blue Light-Emitting Polymers with Fluorinated Backbone for Enhanced Color Purity and Efficiency. *Polymer (Guildf)*. **2012**, *53* (7), 1529–1534.
- (6) Roberts, M.; Asada, K.; Cass, M.; Coward, C.; King, S.; Lee, A.; Pintani, M.; Ramon, M.; Foden, C. Fundamental Processes Governing Operation and Degradation in State of the Art P-OLEDs. *Proc. SPIE* **2010**, *7722*, 77220C.
- (7) Laaperi, A. OLED Lifetime Issues from a Mobile-Phone-Industry Point of View. *J. Soc.*

- Inf. Disp.* **2008**, *16* (11), 1125–1130.
- (8) Poplavskyy, D.; Nelson, J.; Bradley, D. D. C. Ohmic Hole Injection in poly(9,9-Dioctylfluorene) Polymer Light-Emitting Diodes. *Appl. Phys. Lett.* **2003**, *83* (4), 707.
- (9) Song, M. H.; Kabra, D.; Wenger, B.; Friend, R. H.; Snaith, H. J. Optically-Pumped Lasing in Hybrid Organic-Inorganic Light-Emitting Diodes. *Adv. Funct. Mater.* **2009**, *19* (13), 2130–2136.
- (10) Grice, A. W.; Bradley, D. D. C.; Bernius, M. T.; Inbasekaran, M.; Wu, W. W.; Woo, E. P. High Brightness and Efficiency Blue Light-Emitting Polymer Diodes. *Appl. Phys. Lett.* **1998**, *73* (5), 629–631.
- (11) Neher, D. Polyfluorene Homopolymers: Conjugated Liquid-Crystalline Polymers for Bright Blue Emission and Polarized Electroluminescence. *Macromol. Rapid Commun.* **2001**, *22* (17), 1365–1385.
- (12) List, E. J. W.; Guentner, R.; Scanducci de Freitas, P.; Scherf, U. The Effect of Keto Defect Sites on the Emission Properties of Polyfluorene-Type Materials. *Adv. Mater.* **2002**, *14* (5), 374–378.
- (13) Sims, M.; Bradley, D. D. C.; Ariu, M.; Koeberg, M.; Asimakis, A.; Grell, M.; Lidzey, D. G. Understanding the Origin of the 535 Nm Emission Band in Oxidized poly(9,9-Dioctylfluorene): The Essential Role of Inter-Chain/inter-Segment Interactions. *Adv. Funct. Mater.* **2004**, *14* (8), 765–781.
- (14) Bradley, D. D. C.; Grell, M.; Long, X.; Mellor, H.; Grice, A.; Road, H.; Inbasekaran, M.;

- Woo, E. P. Influence of Aggregation on the Optical Properties of a Polyfluorene. *Proc. SPIE* **1997**, *3145*, 254–259.
- (15) Sims, M.; Zheng, K.; Quiles, M. C.; Xia, R.; Stavrinou, P. N.; Bradley, D. D. C.; Etchegoin, P. On the Use of Optical Probes to Monitor the Thermal Transitions in Spin-Coated poly(9,9-Dioctylfluorene) Films. *J. Phys. Condens. Matter* **2005**, *17* (41), 6307–6318.
- (16) Chen, S. H.; Su, A. C.; Chen, S. A. Noncrystalline Phases in poly(9,9-Di-N-Octyl-2,7-Fluorene). *J. Phys. Chem. B* **2005**, *109* (20), 10067–10072.
- (17) Chen, S. H.; Su, A. G.; Su, C. H.; Chen, S. A. Crystalline Forms and Emission Behavior of poly(9,9-Di-N-Octyl-2,7-Fluorene). *Macromolecules* **2005**, *38* (2), 379–385.
- (18) Ariu, M.; Lidzey, D. G.; Lavrentiev, M.; Bradley, D. D. C.; Jandke, M.; Strohriegl, P. A Study of the Different Structural Phases of the Polymer Poly (9,9'-Dioctyl Fluorene) Using Raman Spectroscopy. *Synth. Met.* **2001**, *116*, 217–221.
- (19) Grell, M.; Bradley, D. D. C.; Inbasekaran, M.; Woo, E. P. A Glass-Forming Conjugated Main-Chain Liquid Crystal Polymer for Polarized Electroluminescence Applications. *Adv. Mater.* **1997**, *9* (10), 798–802.
- (20) Grell, M.; Bradley, D. D. C.; Long, X.; Chamberlain, T.; Inbasekaran, M.; Woo, E. P.; Soliman, M. Chain Geometry, Solution Aggregation and Enhanced Dichroism in the Liquid Crystalline Conjugated Polymer poly(9,9-Dioctylfluorene). *Acta Polym.* **1998**, *49* (8), 439–444.

- (21) Grell, M.; Bradley, D. D. C.; Ungar, G.; Hill, J.; Whitehead, K. S. Interplay of Physical Structure and Photophysics for a Liquid Crystalline Polyfluorene. *Macromolecules* **1999**, *32*, 5810–5817.
- (22) Perevedentsev, A.; Chander, N.; Kim, J.-S.; Bradley, D. D. C. Spectroscopic Properties of poly(9,9-Dioctylfluorene) Thin Films Possessing Varied Fractions of β -Phase Chain Segments: Enhanced Photoluminescence Efficiency via Conformation Structuring. *J. Polym. Sci. Part B Polym. Phys.* **2016**, *54*, 1995–2006.
- (23) Perevedentsev, A.; Sonnefraud, Y.; Belton, C. R.; Sharma, S.; Cass, A. E. G.; Maier, S. A.; Kim, J.-S.; Stavrinou, P. N.; Bradley, D. D. C. Dip-Pen Patterning of poly(9,9-Dioctylfluorene) Chain-Conformation-Based Nano-Photonic Elements. *Nat. Commun.* **2015**, *6*, 1–9.
- (24) Ariu, M.; Lidzey, D. G.; Sims, M.; Cadby, A. J.; Lane, P. A.; Bradley, D. D. C. The Effect of Morphology on the Temperature-Dependent Photoluminescence Quantum Efficiency of the Conjugated Polymer poly(9, 9-Dioctylfluorene). *J. Phys. Condens. Matter* **2002**, *14*, 9975–9986.
- (25) Cadby, A. J.; Lane, P. A.; Mellor, H.; Martin, S. J.; Grell, M.; Giebeler, C.; Bradley, D. D. C.; Wohlgenannt, M.; An, C.; Vardeny, Z. V. Film Morphology and Photophysics of Polyfluorene. *Phys. Rev. B* **2000**, *62* (23), 15604–15609.
- (26) Winokur, M.; Slinker, J.; Huber, D. Structure, Photophysics, and the Order-Disorder Transition to the β Phase in poly(9,9-(Di-N,n-Octyl)fluorene). *Phys. Rev. B* **2003**, *67* (18), 184106.

- (27) Ariu, M.; Sims, M.; Rahn, M. D.; Hill, J.; Fox, A. M.; Lidzey, D. G.; Oda, M.; Cabanillas-Gonzalez, J.; Bradley, D. D. C. Exciton Migration in β -Phase poly(9,9-Dioctylfluorene). *Phys. Rev. B* **2003**, *67* (19), 195333.
- (28) Khan, A. L. T.; Sreearunothai, P.; Herz, L. M.; Banach, M. J.; Köhler, A. Morphology-Dependent Energy Transfer within Polyfluorene Thin Films. *Phys. Rev. B* **2004**, *69* (8), 85201.
- (29) Prins, P.; Grozema, F. C.; Nehls, B. S.; Farrell, T.; Scherf, U.; Siebbeles, L. D. A. Enhanced Charge-Carrier Mobility in β -Phase Polyfluorene. *Phys. Rev. B* **2006**, *74* (11), 113203.
- (30) Lu, H. H.; Liu, C. Y.; Chang, C. H.; Chen, S. A. Self-Dopant Formation in poly(9,9-Di-N-Octylfluorene) via a Dipping Method for Efficient and Stable Pure-Blue Electroluminescence. *Adv. Mater.* **2007**, *19* (18), 2574–2579.
- (31) Liang, J.; Yu, L.; Sen Zhao; Ying, L.; Liu, F.; Yang, W.; Peng, J.; Cao, Y. Improving Efficiency and Color Purity of poly(9,9-Dioctylfluorene) through Addition of a High Boiling-Point Solvent of 1-Chloronaphthalene. *Nanotechnology* **2016**, *27* (28), 284001.
- (32) Bai, Z.; Liu, Y.; Li, T.; Li, X.; Liu, B.; Liu, B.; Lu, D. Quantitative Study on β -Phase Heredity Based on Poly(9,9-Dioctylfluorene) from Solutions to Films and the Effect on Hole Mobility. *J. Phys. Chem. C* **2016**, *120* (49), 27820–27828.
- (33) Peet, J.; Brocker, E.; Xu, Y.; Bazan, G. C. Controlled β -Phase Formation in poly(9,9-Di-N-Octylfluorene) by Processing with Alkyl Additives. *Adv. Mater.* **2008**, *20* (10), 1882–1885.

- (34) Tsoi, W. C.; Buckley, A. R.; Lidzey, D. G. Probing the Transitions between Morphological Phases in an Oligofluorene Thin-Film Using Temperature-Dependent Photoluminescence Spectroscopy. *Chem. Phys. Lett.* **2009**, *468*, 32–36.
- (35) Hill, J.; Heriot, S. Y.; Worsfold, O.; Richardson, T. H.; Fox, A. M.; Bradley, D. D. C. Controlled Förster Energy Transfer in Emissive Polymer Langmuir-Blodgett Structures. *Phys. Rev. B* **2004**, *69* (4), 41303.
- (36) Wilkinson, C. I.; Lidzey, D. G.; Palilis, L. C.; Fletcher, R. B.; Martin, S. J.; Wang, X. H.; Bradley, D. D. C. Enhanced Performance of Pulse Driven Small Area Polyfluorene Light Emitting Diodes. *Appl. Phys. Lett.* **2001**, *79* (2), 171–173.
- (37) Chen, L.; Degenaar, P.; Bradley, D. D. C. Polymer Transfer Printing: Application to Layer Coating, Pattern Definition, and Diode Dark Current Blocking. *Adv. Mater.* **2008**, *20* (9), 1679–1683.
- (38) Khan, R. U. A.; Poplavskyy, D.; Kreouzis, T.; Bradley, D. D. C. Hole Mobility within Arylamine-Containing Polyfluorene Copolymers: A Time-of-Flight Transient-Photocurrent Study. *Phys. Rev. B* **2007**, *75* (3), 35215.
- (39) Brewer, P. J.; DeMello, A. J.; DeMello, J. C.; Lane, P. A.; Bradley, D. D. C.; Fletcher, R.; O'Brien, J. Influence of Carrier Injection on the Electromodulation Response of Trap-Rich Polymer Light-Emitting Diodes. *J. Appl. Phys.* **2006**, *99* (11), 114502.
- (40) Redecker, M.; Bradley, D. D. C.; Inbasekaran, M.; Wu, W. W.; Woo, E. P. High Mobility Hole Transport Fluorene-Triarylamine Copolymers. *Adv. Mater.* **1999**, *11* (3), 241–246.

- (41) Campbell, A. J.; Bradley, D. D. C.; Antoniadis, H.; Inbasekaran, M.; Wu, W. S. W.; Woo, E. P. Transient and Steady-State Space-Charge-Limited Currents in Polyfluorene Copolymer Diode Structures with Ohmic Hole Injecting Contacts. *Appl. Phys. Lett.* **2000**, 76 (13), 1734–1736.
- (42) Janietz, S.; Bradley, D. D. C.; Grell, M.; Giebeler, C.; Inbasekaran, M.; Woo, E. P. Electrochemical Determination of the Ionization Potential and Electron Affinity of poly(9,9-Dioctylfluorene). *Appl. Phys. Lett.* **1998**, 73 (17), 2453–2455.
- (43) Sekine, C.; Tsubata, Y.; Yamada, T.; Kitano, M.; Doi, S. Recent Progress of High Performance Polymer OLED and OPV Materials for Organic Printed Electronics. *Sci. Technol. Adv. Mater.* **2014**, 15 (3), 34203.
- (44) Lu, L. P.; Kabra, D.; Johnson, K.; Friend, R. H. Charge-Carrier Balance and Color Purity in Polyfluorene Polymer Blends for Blue Light-Emitting Diodes. *Adv. Funct. Mater.* **2012**, 22 (1), 144–150.
- (45) Campbell, A. J.; Rawcliffe, R.; Guite, A.; Faria, J. C. D.; Mukherjee, A.; Mclachlan, M. A.; Shkunov, M.; Bradley, D. D. C. Charge-Carrier Density Independent Mobility in Amorphous Fluorene-Triarylamine Copolymers. *Adv. Funct. Mater.* **2016**, 3720–3729.
- (46) Liu, B.; Lin, J.; Liu, F.; Yu, M.; Zhang, X.; Xia, R.; Yang, T.; Fang, Y.; Xie, L.; Huang, W. A Highly Crystalline and Wide-Bandgap Polydiarylfluorene with β -Phase Conformation toward Stable Electroluminescence and Dual Amplified Spontaneous Emission. *ACS Appl. Mater. Interfaces* **2016**, 8 (33), 21648–21655.
- (47) Tsoi, W. C.; Charas, A.; Cadby, A. J.; Khalil, G.; Adawi, A. M.; Iraqi, A.; Hunt, B.;

- Morgado, J.; Lidzey, D. G. Observation of the β -Phase in Two Short-Chain Oligofluorenes. *Adv. Funct. Mater.* **2008**, *18* (4), 600–606.
- (48) Ryu, G.; Stavrinou, P. N.; Bradley, D. D. C. Spatial Patterning of the β -Phase in poly(9,9-Dioctylfluorene): A Metamaterials-Inspired Molecular Conformation Approach to the Fabrication of Polymer Semiconductor Optical Structures. *Adv. Funct. Mater.* **2009**, *19* (20), 3237–3242.
- (49) Tamai, Y.; Ohkita, H.; Bente, H.; Ito, S. Triplet Exciton Dynamics in Fluorene – Amine Copolymer Films. *Chem. Mater.* **2014**, *26*, 2733–2742.
- (50) Richards, C. E.; Phillips, R. T. Solvatochromic Effects on the Photoinduced Charge-Transfer States in Donor-Acceptor Substituted Polydioctylfluorenes. *ChemPhysChem* **2011**, *12* (15), 2831–2835.
- (51) Cerullo, G.; Stagira, S.; Zavelani-Rossi, M.; De Silvestri, S.; Virgili, T.; Lidzey, D. G.; Bradley, D. D. C. Ultrafast Forster Transfer Dynamics in Tetraphenylporphyrin Doped poly(9,9-Dioctylfluorene). *Chem. Phys. Lett.* **2001**, *335* (1–2), 27–33.
- (52) Buckley, A. R.; Rahn, M. D.; Hill, J.; Cabanillas-Gonzalez, J.; Fox, A. M.; Bradley, D. D. C. Energy Transfer Dynamics in Polyfluorene-Based Polymer Blends. *Chem. Phys. Lett.* **2001**, *339* (5–6), 331–336.
- (53) Becker, K.; Lupton, J. M.; Feldmann, J.; Nehls, B. S.; Galbrecht, F.; Gao, D. Q.; Scherf, U. On-Chain Fluorenone Defect Emission from Single Polyfluorene Molecules in the Absence of Intermolecular Interactions. *Adv. Funct. Mater.* **2006**, *16* (3), 364–370.

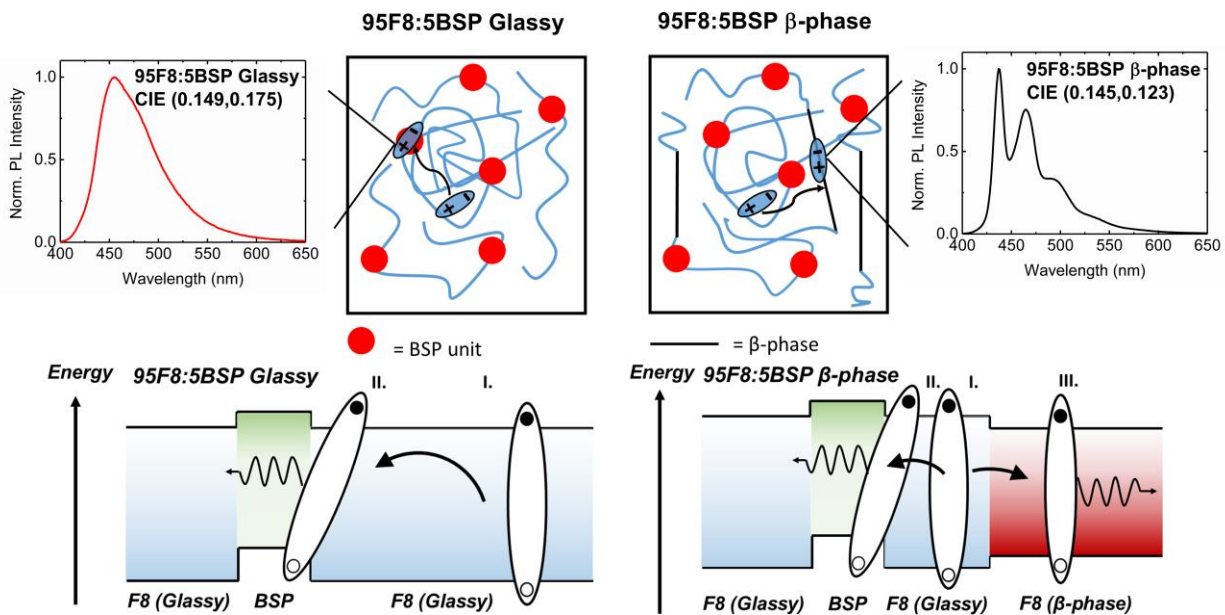
- (54) Arredondo, B.; Romero, B.; Gutiérrez-Llorente, A.; Martínez, A. I.; Álvarez, A. L.; Quintana, X.; Otón, J. M. On the Electrical Degradation and Green Band Formation in α -And β -Phase poly(9,9-Dioctylfluorene) Polymer Light-Emitting Diodes. *Solid. State. Electron.* **2011**, *61* (1), 46–52.
- (55) Monkman, A.; Rothe, C.; King, S.; Dias, F. Polyfluorene Photophysics. *Adv. Polym. Sci.* **2008**, *212* (1), 187–225.
- (56) Redecker, M.; Bradley, D. D. C.; Baldwin, K. J.; Smith, D. A.; Inbasekaran, M.; Wu, W. W.; Woo, E. P. An Investigation of the Emission Solvatochromism of a Fluorene-Triarylamine Copolymer Studied by Time Resolved Spectroscopy. *J. Mater. Chem.* **1999**, *9* (9), 2151–2154.
- (57) Hooley, E. N.; Jones, D. J.; Greenham, N. C.; Ghiggino, K. P.; Bell, T. D. M. Charge Transfer in Single Chains of a Donor-Acceptor Conjugated Tri-Block Copolymer. *J. Phys. Chem. B* **2015**, *119* (24), 7266–7274.
- (58) Morteani, A. C.; Friend, R. H.; Silva, C. Endothermic Exciplex-Exciton Energy-Transfer in a Blue-Emitting Polymeric Heterojunction System. *Chem. Phys. Lett.* **2004**, *391* (1–3), 81–84.
- (59) Zhang, X.; Lei, Z.; Hu, Q.; Lin, J.; Chen, Y.; Xie, L.; Lai, W.; Huang, W. Stable Pure-Blue Polymer Light-Emitting Devices Based on β -Phase poly(9,9-Dioctylfluorene) Induced by 1,2-Dichloroethane. *Appl. Phys. Express* **2014**, *7*, 101601.
- (60) Yao, B.; Zhang, B.; Ding, J.; Xie, Z.; Zhang, J.; Wang, L. Direct Formation of β Phase in Polyoctylfluorene Thin Film via Solvent Vapor Assisted Spin-Coating Method. *Org.*

Electron. **2013**, *14* (3), 897–901.

- (61) Chan, K. L.; Sims, M.; Pascu, S. I.; Ariu, M.; Holmes, A. B.; Bradley, D. D. C. Understanding the Nature of the States Responsible for the Green Emission in Oxidized poly(9,9-Dialkylfluorene)s: Photophysics and Structural Studies of Linear Dialkylfluorene/fluorenone Model Compounds. *Adv. Funct. Mater.* **2009**, *19* (13), 2147–2154.
- (62) Xia, C.; Advincula, R. C. Decreased Aggregation Phenomena in Polyfluorenes by Introducing Carbazole Copolymer Units. *Macromolecules* **2001**, *34* (17), 5854–5859.
- (63) Miteva, T.; Meisel, A.; Knoll, W.; Nothofer, H. G.; Scherf, U.; Müller, D. C.; Meerholz, K.; Yasuda, A.; Neher, D. Improving the Performance of Polyfluorene-Based Organic Light-Emitting Diodes via End-Capping. *Adv. Mater.* **2001**, *13* (8), 565–570.
- (64) Campbell, A. J.; Bradley, D. D. C.; Virgili, T.; Lidzey, D. G.; Antoniadis, H. Improving Efficiency by Balancing Carrier Transport in poly(9,9-Dioctylfluorene) Light-Emitting Diodes Using Tetraphenylporphyrin as a Hole-Trapping, Emissive Dopant. *Appl. Phys. Lett.* **2001**, *79* (23), 3872–3874.
- (65) Montilla, F.; Ruseckas, A.; Samuel, I. D. W. Absorption Cross-Sections of Hole Polarons in Glassy and β -Phase Polyfluorene. *Chem. Phys. Lett.* **2013**, *585*, 133–137.
- (66) Bradley, D. D. C.; Friend, R. H. Light-Induced Luminescence Quenching in Precursor-Route Poly(p-Phenylene Vinylene). *J. Phys. Condens. Matter* **1989**, *1*, 3671–3678.
- (67) Morteani, A. C.; Dhoot, A. S.; Kim, J.-S.; Silva, C.; Greenham, N. C.; Murphy, C.;

Moons, E.; Ciná, S.; Burroughes, J. H.; Friend, R. H. Barrier-Free Electron–Hole Capture in Polymer Blend Heterojunction Light-Emitting Diodes. *Adv. Mater.* **2003**, *15* (20), 1708–1712.

TABLE OF CONTENTS IMAGE



Supporting Information

Controlling Molecular Conformation for Highly Efficient and Stable Deep-Blue Copolymer Light-Emitting Diodes

Iain Hamilton,[†] Nathan Chander,[†] Nathan J. Cheetham,[†] Minwon Suh,[†] Matthew Dyson,^{†,§}

Xuhua Wang,[†] Paul N. Stavrinou,[‡] Michael Cass,[⊥] Donal D. C. Bradley,^{‡,||} and Ji-Seon Kim^{*†}*

[†] Department of Physics and Centre for Plastic Electronics, Imperial College London, London SW7 2AZ, UK

[‡] Department of Engineering Science, University of Oxford, Parks Road, Oxford, OX1 3PJ, UK

[§] Molecular Materials and Nanosystems and Institute for Complex Molecular Systems, Eindhoven University of Technology, P.O. Box 513, 5600 MB Eindhoven, The Netherlands

[⊥] Cambridge Display Technology Ltd, Unit 12 Cardinal Park, Godmanchester, Cambridgeshire PE29 2XG, UK

^{||} Department of Physics and Division of Mathematical, Physical and Life Sciences, University of Oxford, 9 Parks Road, Oxford, OX1 3PD, UK

^{*} ji-seon.kim@imperial.ac.uk, Donal.Bradley@mpls.ox.ac.uk

Contents

β -phase fraction calculation.....	S-53
--	------

Uv-vis and PL spectra for 97F8:3BSP, 90F8:10BSP, 80F8:20BSP and PFB copolymer films	S-56
Solvatochromism in PFO, 95F8:5BSP and PFB	S-59
Cyclic Voltammetry	S-60
Deconvoluted photoluminescence spectra	S-63
Overlaid UV-vis absorbance and photoluminescence spectra for glassy- and β -phase PFO, 95F8:5BSP copolymer and 90PFO/10PFB blend films.....	S-65
Time-correlated-single-photon-counting (TCSPC) PL decay measurements for PFO, 95F8:5BSP, 90PFO/10PFB and PFB.....	S-66
Solution TCSPC measurements	S-69
Deconvoluted electroluminescence spectra for 95F8:5BSP copolymer and 90PFO/10PFB blend β -phase EML devices.....	S-70
AFM Topography images	S-71
97F8:3BSP and 90F8:10BSP copolymer PLED device data.....	S-74
95F8:5BSP PLED device lifetime	S-78
Low temperature photoluminescence measurements	S-80
Voltage dependent EL spectra for a ~95 nm thick 95F8:5BSP β -phase PLED	S-82
Energy transfer mechanism in 90PFO/10PFB blend films and PLEDs	S-33
References	S-84

β-phase fraction calculation

The absorption spectra of the homopolymer (PFO), copolymer (nF8:mBSP) and blend (xPFO/yPFB) films can be described as a superposition of the absorption of disordered glassy-phase (broad peak centred at ≈ 385 nm) and well-ordered β-phase (resolved vibronic band with S_0 - S_1 0-0 peak at ≈ 435 nm) chain segments. To estimate the fraction of β-phase chain segments in each film, the appropriate reference ‘purely-glassy’ absorption spectrum (blue dashed line in Figure S1) is fitted at 3.55 eV where there is negligible β-phase segment absorption.^{S1} The thus-normalised glassy spectrum is then subtracted from the film spectrum and the residual corresponds to the β-phase chain segment absorption (red dashed line). The fraction of β-phase segments in the film can then be estimated from the ratio of the integrated absorption areas after taking into account the enhanced oscillator strength for β-phase segments (a factor of 1.08).^{S1}

$$\beta\text{-phase fraction (\%)} = \frac{\Delta A}{\Delta A + \{(A_{\text{total}} - \Delta A) \times 1.08\}} \times 100$$

In the examples shown in Figure S1 we estimate (from top to bottom) 10, 5 and 12% β-phase chain segments.

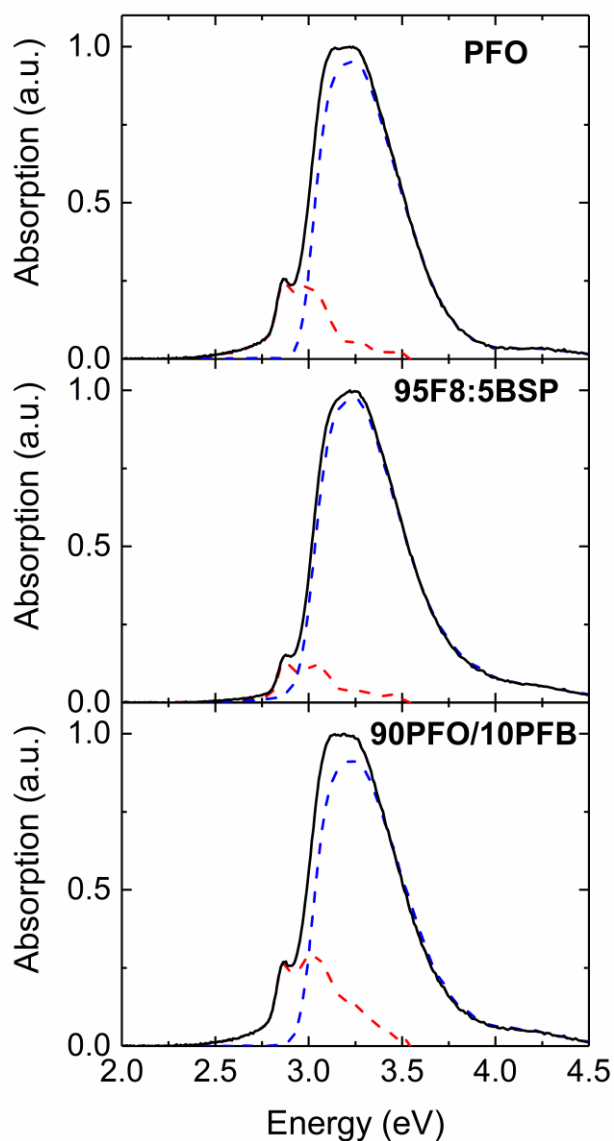


Figure S1. Normalised absorption spectra of homopolymer PFO, copolymer 95F8:5BSP and blend 90PFO/10PFB β -phase films (black solid line). In each case, a ‘purely-glassy’ film spectrum (blue dashed lines) is overlaid. The difference spectra correspond to the β -phase segment absorptions (red).

A higher fraction of β -phase chain segments is formed in films of the PFO homopolymer (10%) and 90PFO/10PFB blend (12%) than in films of the 95F8:5BSP copolymer (5%). The

effect that PFB chains have on neighbouring PFO chain motions in blend films is difficult to predict *a priori*. Both disruptive (motion constraining) and assistive (free-volume generating) effects might occur and their balance will influence the degree to which β -phase conformations can be adopted by the PFO fraction. Further studies will be required to investigate this behaviour in detail but we note that here the overall effect of forming a blend with 10% PFB is marginally beneficial to β -phase generation. In contrast, for the 95F8:5BSP copolymer, the BSP moieties are present within all of the chains and the smaller fraction of β -phase chain segments observed following SVA then suggests that in this case they tend to impede β -phase formation.

UV-vis and PL spectra for 97F8:3BSP, 90F8:10BSP, 80F8:20BSP and PFB copolymer films

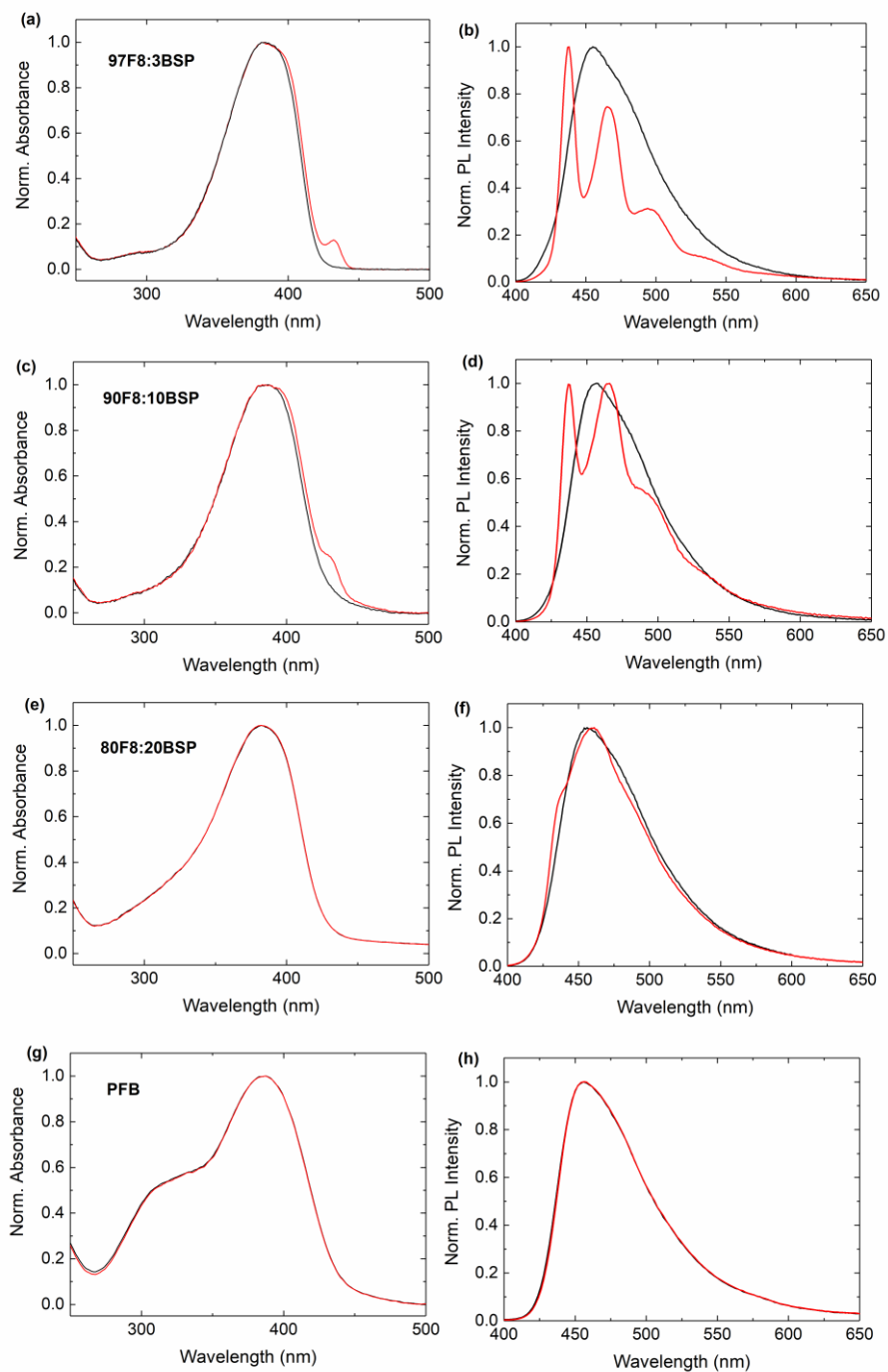


Figure S2. UV-vis absorption (left column) and PL spectra (right column) for pre- (black line) and post- (red line) solvent-vapour-annealed copolymer films of 97F8:3BSP ((a) and (b)), 90F8:10BSP ((c) and (d)), 80F8:20BSP ((e) and (f)) and 50F8:50BSP (PFB) ((g) and (h)).

Table S1. Comparison of β -phase fraction and β -phase PL contribution for solvent vapour annealed 97F8:3BSP, 90F8:10BSP, 80F8:20BSP and PFB copolymer films determined by fitting the data shown in Figure S2.

<i>Polymer</i>	<i>β-phase fraction</i>	<i>β-phase PL contribution</i>
<i>97F8:3BSP</i>	6% \pm 1%	69%
<i>90F8:10BSP</i>	3% \pm 1%	46%
<i>80F8:20BSP</i>	0.2% \pm 0.1%	8%
<i>PFB (50F8:50BSP)</i>	0%	0%

The formation of β -phase chain segments was investigated for further F8:BSP statistical copolymer compositions, namely 97F8:3BSP, 90F8:10BSP and 80F8:20BSP with 3%, 10% and 20% of butyl substituted phenylenediamine (BSP) units, and for PFB, the 50F8:50BSP alternating copolymer. Figure S2 shows their thin film UV-vis and PL spectra before and after solvent vapour annealing (SVA) using the same conditions outlined in the experimental section of the main paper. The 97F8:3BSP copolymer forms 6% β -phase chain segments but this gives rise to 69% of the PL emission. SVA of the 90F8:10BSP copolymer yields a smaller fraction of β -phase segments (3%) but again, this is disproportionately represented in the emission, with a 46% β -phase PL contribution. Interestingly, the 80F8:20BSP copolymer still shows a small amount of β -phase when in fact none would be expected were the BSP units evenly distributed amongst the polymer chains. Four F8 units between each BSP unit would be too short a sequence

to support β -phase segment formation. The very small (0.2%) fraction of β -phase segments is again over-represented in PL with an 8% fraction in emission. Lastly, it is confirmed that, as expected, β -phase segments cannot form in the alternating copolymer (PFB).

Solvatochromism in PFO, 95F8:5BSP and PFB

Figure S3 shows the effect of solvent polarity (toluene vs THF vs dichlorobenzene) on the solution PL spectra for PFO, PFB and 95F8:5BSP. Very small spectral shifts are seen for the vibronically structured PFO PL consistent with neutral exciton emission. For PFB the PL shifts are substantially larger, as expected for excited states with charge transfer (CT) character. For 95F8:5BSP the emission has both neutral exciton and CT-like components that show a combination of PFO- and PFB-like behaviours.

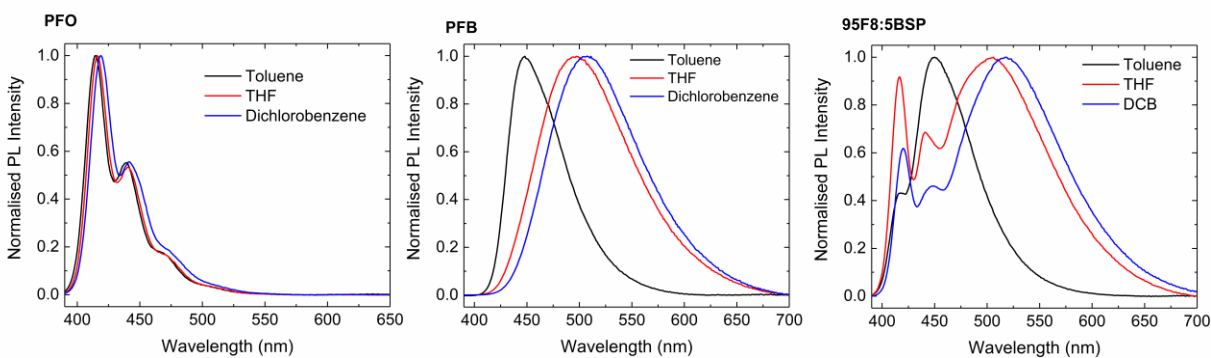


Figure S3. PL spectra of PFO, PFB and 95F8:5BSP in dilute Toluene, THF and Dichlorobenzene solutions.

Cyclic Voltammetry

For reference in the discussion of energy transfer processes occurring in the homopolymer, copolymer and blend films, the HOMO and LUMO levels of PFO, 95F8:5BSP and PFB were determined using cyclic voltammetry (CV). Films were prepared by spin coating onto ITO substrates that acted as the working electrode in a traditional three-electrode setup. A platinum wire was used as the auxiliary electrode and Ag/Ag⁺ as reference electrode. The measurements (scan rate 100 mV/s) were carried out using a 0.1M tetrabutylammonium hexafluorophosphate (TBAPF₆) acetonitrile solution for both oxidation and reduction, and recorded using an Autolab PGSTAT101 instrument. For the CV measurements in acetonitrile, the glassware was dried at 100 °C and the cell purged with argon during the measurement to prevent oxygen contamination.

The measurement was calibrated by collecting a CV scan for ferrocene, with its known ionisation potential of 4.8 eV. The corresponding half wave potential ($E_{1/2}$) for Fe/Fe⁺ was measured to be 0.40 eV in our setup, yielding:

$$E_{\text{HOMO}} = (E_{\text{ox}} + 4.40 \text{ eV})$$

$$E_{\text{LUMO}} = (E_{\text{red}} + 4.40 \text{ eV})$$

Where E_{ox} and E_{red} are the onset voltages for oxidation and reduction respectively.

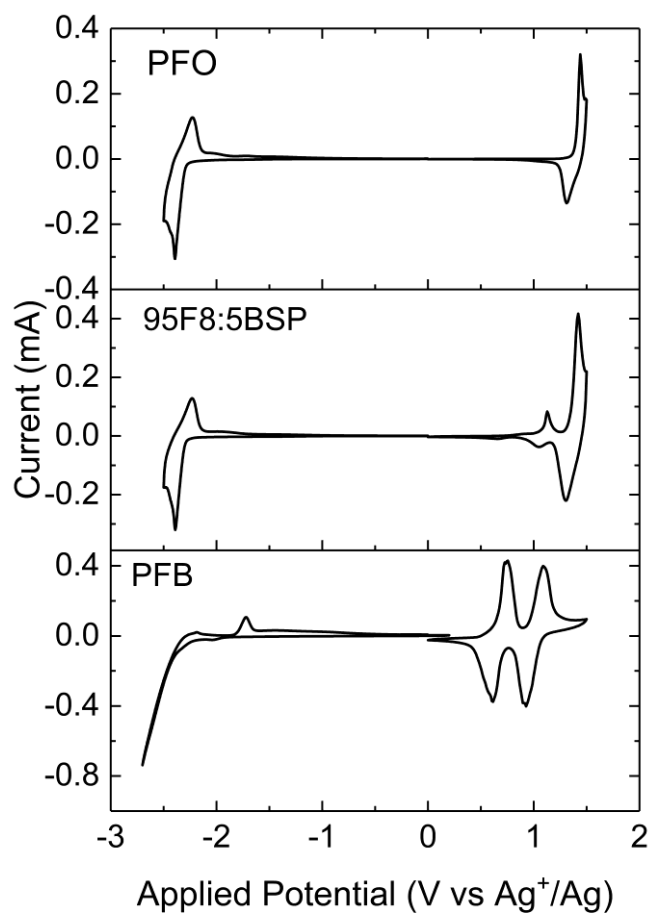


Figure S4. Cyclic voltammograms for thin film samples of (a) PFO, (b) 95F8:5BSP and (c) PFB recorded in TBAPF₆ acetonitrile solution.

Table S2. Table showing values of oxidation onset energy, reduction onset energy and estimated HOMO and LUMO energies for PFO, 95F8:5BSP and PFB.

Polymer	E _{ox} (eV)	E _{red} (eV)	HOMO (eV)	LUMO (eV)
PFO	1.40	-2.30	5.80	2.10
F8:BSP 95:5	1.09	-2.30	5.49	2.10
PFB	0.65	-2.40	5.05	2.00

A spatial separation of electron and hole wavefunctions is supported by cyclic voltammetry (CV) measurements (Figure S4). For 95F8:5BSP a small oxidation peak is observed at ~ 0.3 V below the main F8 oxidation peak. This can be assigned to preferential oxidation of BSP moieties confirming HOMO localization at these sites. Conversely, the LUMO will tend to delocalize across extended F8 sequences.^{S2} The introduction of BSP moieties can thereby lead to hole trapping and enhanced exciton formation in PLEDs.^{S3}

Deconvoluted photoluminescence spectra

The PL spectra were deconvoluted to determine the contribution of β -phase F8 segments to the PL emission. Here, the 95F8:5BSP copolymer and 90PFO/10PFB blend β -phase film PL were fitted by the sum of two reference PL spectra. For copolymer β -phase films the reference spectra used were: PL of glassy 95F8:5BSP (dashed red line in left panel of Figure S6) and β -phase PFO (blue dashed lines). For the 90PFO/10PFB blend film, a glassy PFB (50PFO:50BSP) reference was used (red dashed line in right panel of Figure S5) along with the same β -phase PFO spectrum.

The relative magnitudes of the reference spectra were adjusted so that the sum (black solid line in Figure S6) gave a good fit to the measured β -phase PL spectra (open circles). The relative contribution of the β -phase emission was then found from the ratio of the integrated intensities.

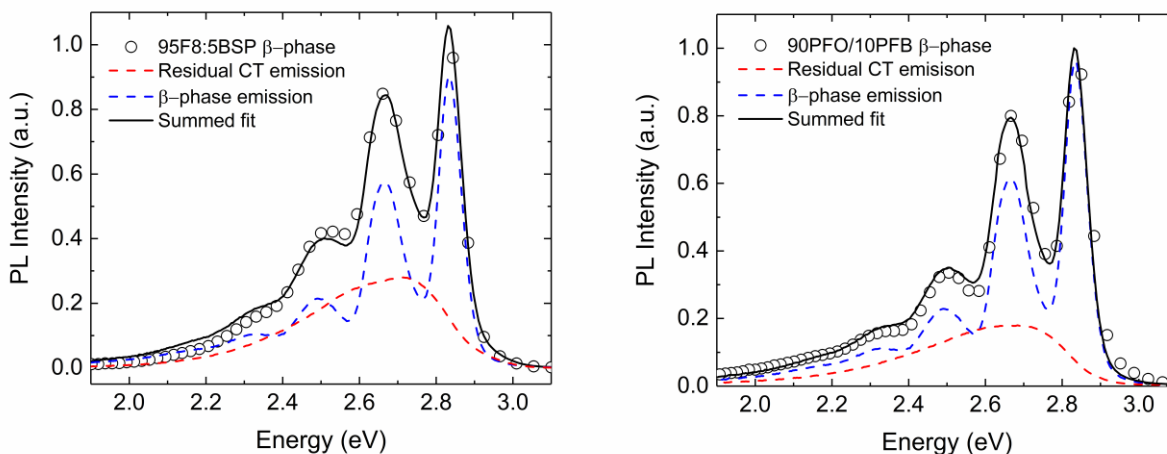


Figure S5. Deconvolution of PL spectra for 95F8:5BSP copolymer β -phase sample (left – open circles) and 90PFO/10PFB blend β -phase sample (right – open circles). The red dashed line shows residual PFB-like CT emission whilst the blue dashed line shows the vibronic β -phase emission. The solid black line shows the combined sum of residual CT and β -phase emissions.

The fractional contribution from each component was deduced by integration over their deconvoluted spectra. For the copolymer, the β -phase fraction accounted for 62% of total emission whilst for the blend, β -phase PFO emission accounted for 82% of the total spectra.

Overlaid UV-vis absorbance and photoluminescence spectra for glassy- and β -phase PFO, 95F8:5BSP copolymer and 90PFO/10PFB blend films

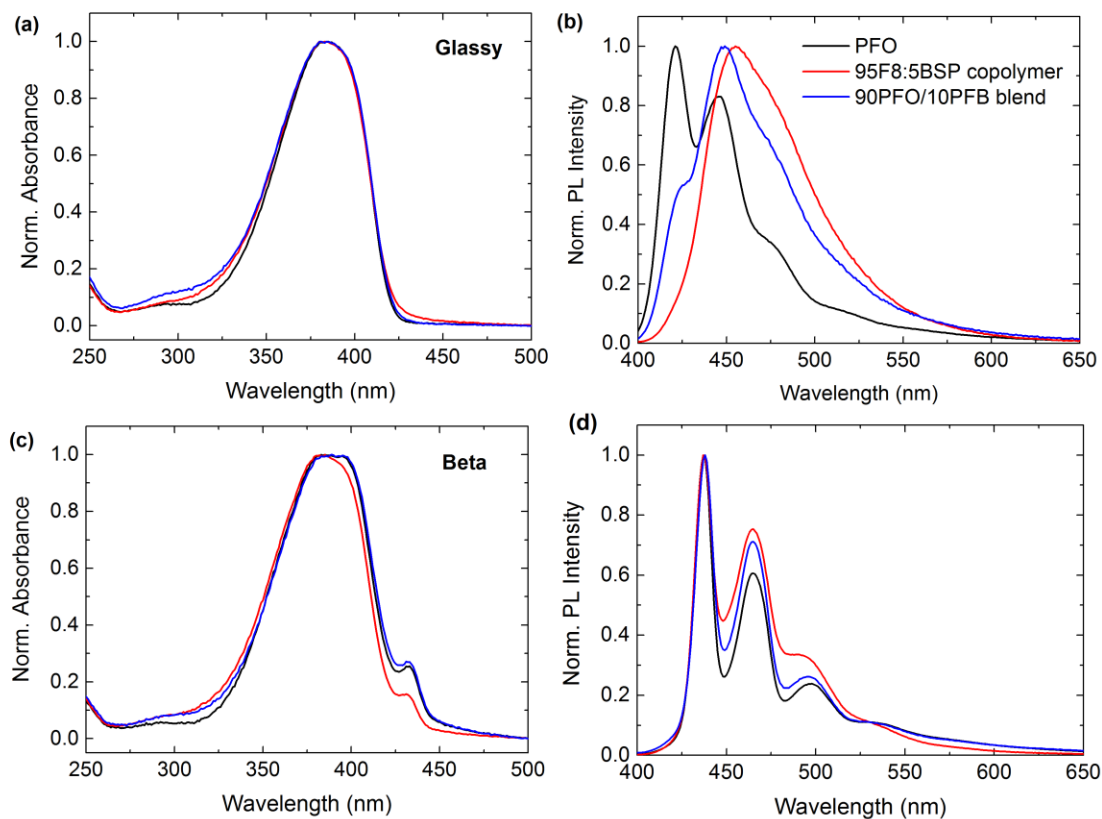


Figure S6. Peak normalised optical absorption ((a) and (c)) and PL emission ($\lambda_{\text{ex}} = 385$ nm) spectra ((b) and (d)) for PFO (black line), 95F8:5BSP copolymer (red line) and 90PFO/10PFB blend (blue line) films spin coated on spectrosil substrates. Glassy-phase data are shown in (a) and (b) whilst β -phase data are shown in (c) and (d). Spectra are overlaid for ease of comparison of the initial glassy-phase differences and the changes arising from β -phase chain segment formation within the three film types.

Time-correlated-single-photon-counting (TCSPC) PL decay measurements for PFO, 95F8:5BSP, 90PFO/10PFB and PFB

Thin film measurements

Figure S7 shows thin film TCSPC measurements ($\lambda_{\text{ex}} = 404 \text{ nm}$) for glassy and β -phase microstructures of PFO, 95F8:5BSP and 90PFO/10PFB blend samples collected at range of wavelengths between 420-540 nm. PFO (glassy and β -phase) shows a bi-exponential decay made up of fast excitonic decay and slower, excimer-like decay from ‘green-band’ fluorenone defects.^{S4} The latter decay increases in proportion at longer wavelength collections.

95F8:5BSP copolymer samples show decay times vary substantially with emission wavelength, with decay times increasing with wavelength collection rather than a change in component amplitude (as in PFO), suggesting a distribution of CT lifetimes within the copolymer.

The glassy 90PFO/10PFB blend sample shows a similar trend to the copolymer case, which is not surprising given that CT states from the PFB make up a significant fraction of the emission. β -phase 90PFO/10PFB TCSPC traces however shows a more PFO-like trend (redistribution of weights rather than lifetime as wavelength collection increases) as now excitonic PFO emission makes up the majority of PL emission.

PFB TCSPC traces (Figure S8) shows decay times increase with emission wavelength, as in the 95F8:5BSP copolymer case.

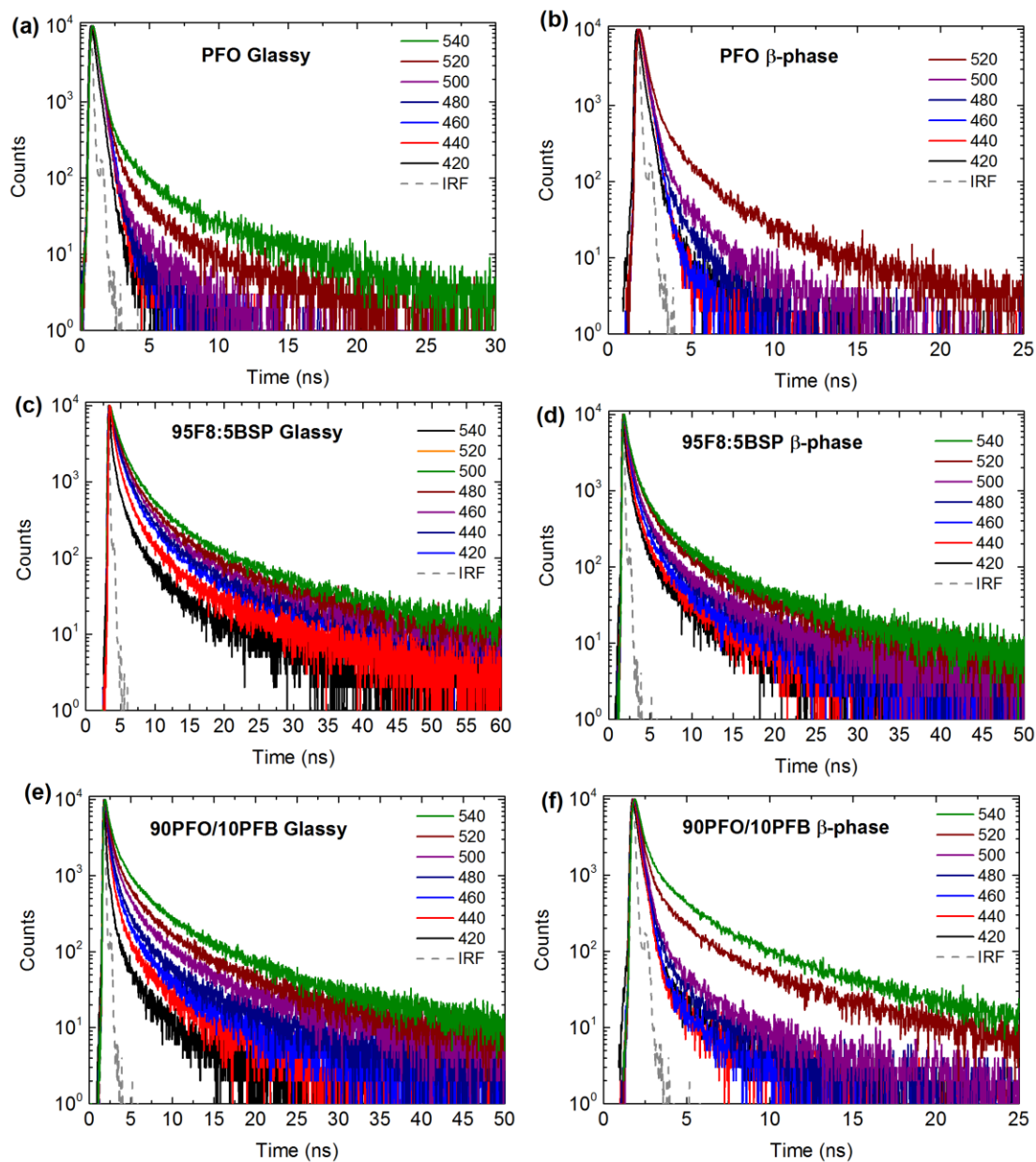


Figure S7. Thin film TCSPC decay curves ($\lambda_{\text{ex}} = 404$ nm) collected for the glassy- (left column) and β -phase (right column) microstructures of PFO ((a) and (b)), 95F8:5BSP ((c) and (d)) and 90PFO/10PFB ((e) and (f)). The dashed line is the instrument response function (IRF) and the decay curves from top to bottom run from long to short wavelengths (see legends for wavelength values in nm).

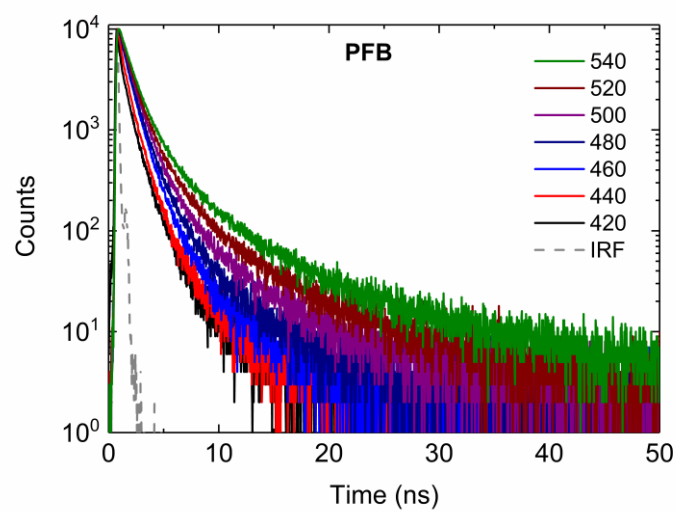


Figure S8. Thin film TCSPC decay curves for PFB. The dashed line is the instrument response function (IRF) and the decay curves from top to bottom run from long to short wavelengths (see legend for wavelength values in nm).

Solution measurements

Figure S9(a) shows the PL spectra of PFO, 95F8:5BSP and PFB in a dilute toluene solution, whilst parts (b)-(d) shows the solution TCSPC decay curves of PFO, 95F8:5BSP and PFB collected at 420-540 nm. PFO and PFB show mono-exponential decays at all collection wavelengths (~ 356 ps for PFO and ~ 1.4 ns for PFB) whilst the PL transients of the 95F8:5BSP copolymer in dilute solution (Figure S9(c)) show a bi-exponential decay at shorter wavelengths (420 and 440 nm), attributed to combined PFO-like excitonic emission (with $\tau_1 \sim 140$ ps) and PFB-like CT emission (with $\tau_2 \sim 1.4$ ns). At longer wavelengths, beyond 460 nm, a mono-exponential decay with $\tau \approx 1.4$ ns is observed, identical to the dilute solution decay for PFB.

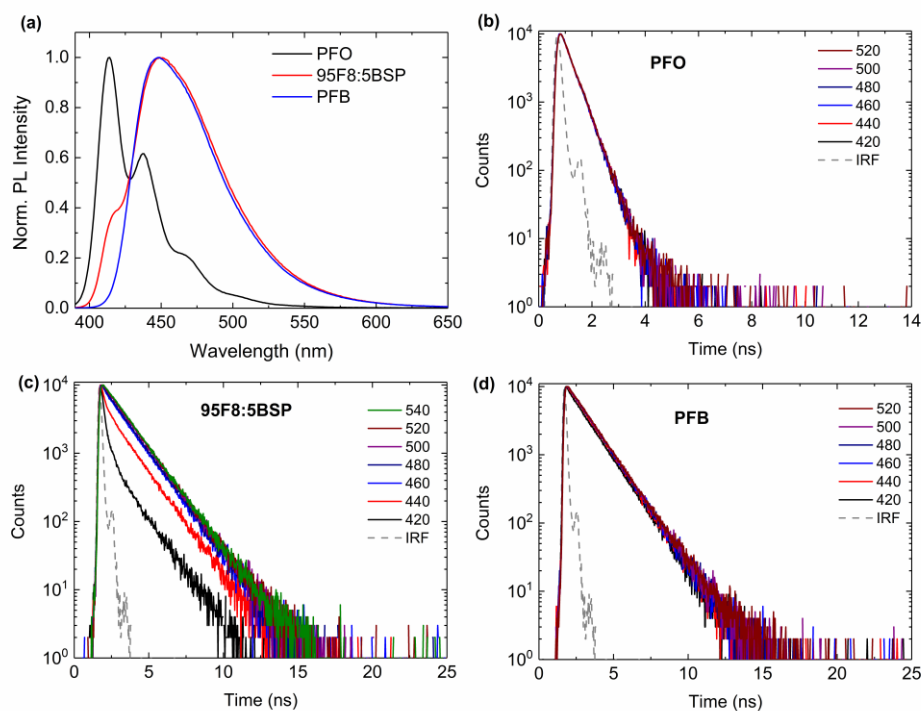


Figure S9. (a) PL emission spectra and ((b), (c), (d)) TCSPC decay curves for PFO, 95F8:5BSP and PFB in dilute (0.05 mg/ml) toluene solution. The homopolymer and alternating copolymer show single exponential decays whilst the sparse copolymer has more complex kinetics consistent with its two-component (PFO-like vibronic plus PFB-like CT) PL emission spectrum.

Deconvoluted electroluminescence spectra for 95F8:5BSP copolymer and 90PFO/10PFB blend β -phase EML devices

As for the PL spectra above, EL spectra from 95F8:5BSP copolymer and 90PFO/10PFB blend β -phase EML devices were deconvoluted to reveal the relative contributions of structured vibronic and CT-like emissions. The same procedure was applied to the EL data as used for PL.

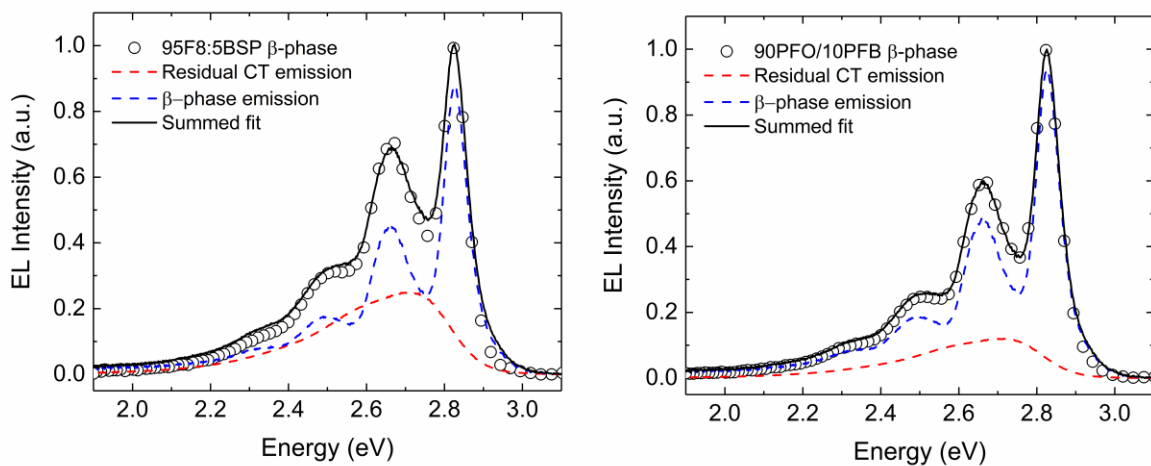


Figure S10. Deconvolution of EL spectra for 95F8:5BSP copolymer β -phase sample (left) and 90PFO/10PFB blend β -phase sample (right). The red dashed line shows residual PFB-like CT emission, whilst the blue dashed line shows the vibronic β -phase emission. The fractional contribution from each component was deduced by integration over their deconvoluted spectra.

AFM Topography images for PFO, 95F8:5BSP copolymer and 90PFO/10BSP blend films

Overall, the performance of the 90PFO/10PFB blend devices is poorer than for the 95F8:5BSP copolymer devices. It is clear that the volume fraction of BSP moieties is not the determining factor in this regard but the distribution of moieties within a polymer chain and through the bulk of a film also matter. In the blend, the BSP moieties are incorporated within PFB polymer chains at high density (alternating with 9,9-dioctylfluorene moieties) and these chains are then mixed with a majority (90%) of PFO polymer chains from which (at least partial) phase separation will occur. Evidence for phase separation is provided by the EL spectrum for glassy blend EML devices that shows a glassy PFO contribution (c.f. shoulder at ~ 425 nm on the blue edge of the spectrum) indicating incomplete energy transfer to PFB CT like emission sites. Atomic force microscopy (AFM) images for 60 nm thickness films of each EML are shown in Figure S11. Whilst the PFO and 95F8:5BSP films show largely featureless thin film microstructures (Figure S11 (a)-(d)), the 90PFO/10PFB blend films do indeed show phase separation between PFB and PFO chains in the glassy phase (Figure S11 (e)), with the image appearing to show ~ 10 nm raised islands through the film with a roughness of 1.32 nm. The β -phase blend thin film microstructure (Figure S11 (f)), however, appears to show ~ 10 nm sized recesses with a roughness of 1.76 nm. This suggests that whilst BSP units are evenly distributed through the 95F8:5BSP copolymer film, in the blend case the PFB chains are segregated, leading to less effective hole trapping which therefore leads to decreased device performance. In addition, β -phase segment formation by SVA has a more substantial effect on the EL spectrum of the blend EML devices than seen for 95F8:5BSP copolymer devices; deconvolution (Figure S10) indicates 80% β -phase emission and 20% CT emission compared to 66% β -phase and 34% CT emission for copolymer EML devices.

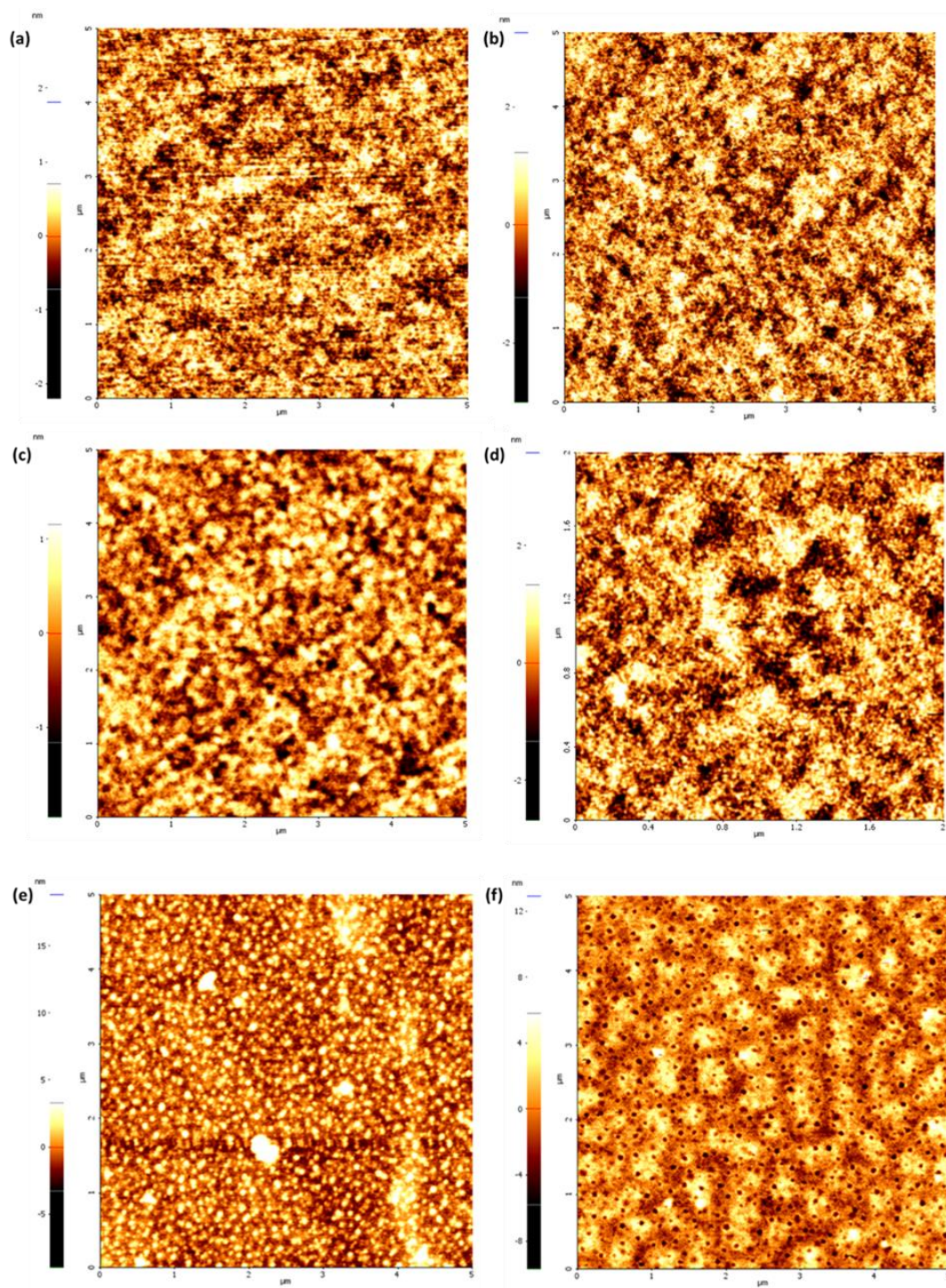


Figure S11. AFM topography images for glassy phase (left column) and β -phase (right column) microstructures of PFO ((a) and (b)), 95F8:5BSP copolymer ((c) and (d)) and 90PFO/10PFB blend ((e) and (f)) films.

Table S3. Root mean square roughness values (R_q) for PFO, 95F8:5BSP copolymer and 90PFO/10PFB blend films with glassy- and β -phase microstructures. The surface roughness for the blend is significantly higher than for the other two films. It is also generally the case that β -phase films are rougher than glassy ones.

Film Type	Roughness, R_q (nm)
PFO Glassy	0.349
PFO β -phase	0.627
95F8:5BSP Glassy	0.459
95F8:5BSP β -phase	0.680
90PFO/10PFB Glassy	1.319
90PFO/10PFB β -phase	1.763

97F8:3BSP and 90F8:10BSP copolymer PLED device data

PLED devices (ITO/PEDOT:PSS/TFB/copolymer EML/LiF/Ca/Al) were fabricated using 97F8:3BSP and 90F8:10BSP with both glassy and β -phase microstructures. J-V-L and efficiency (cd/A and lm/W) vs Voltage data are shown in Figure S13 and peak characteristics extracted therefrom are listed in Table S3. The 97F8:3BSP EMLs give good device performance with peak efficiencies of 3.4 cd/A and 2.4 lm/W for glassy and 3.1 cd/A and 2.0 lm/W for β -phase. The β -phase microstructure yields a slight drop in efficiency consistent with the behaviour for 95F8:5BSP copolymer and 90PFO/10PFB blend devices, however it also yields a desirable blue shift in emission from CIE(x, y) = (0.15, 0.17) to (0.15, 0.13). The EL spectra for both glassy and β -phase 97F8:3BSP EMLs are shown in Figure S14. The β -phase device shows strong S_1 - S_0 vibronic emission with its 0-0 transition at 440 nm.

The 90F8:10BSP EML devices yielded poorer performance than 97F8:3BSP and 95F8:5BSP devices, with efficiencies of 1.7 cd/A and 0.6 lm/W for glassy and 1.3 cd/A and 0.4 lm/W for β -phase. We suggest that the increase in BSP content tends to reduce hole trapping, resulting in an increased hole-leakage current. The luminous efficiencies are again somewhat reduced for β -phase but as before there is a favourable blue shift in CIE (x, y) from (0.15, 0.16) to (0.15, 0.15); albeit that in this case the effect is less strong due to the lower fraction of vibronic emission that arises.

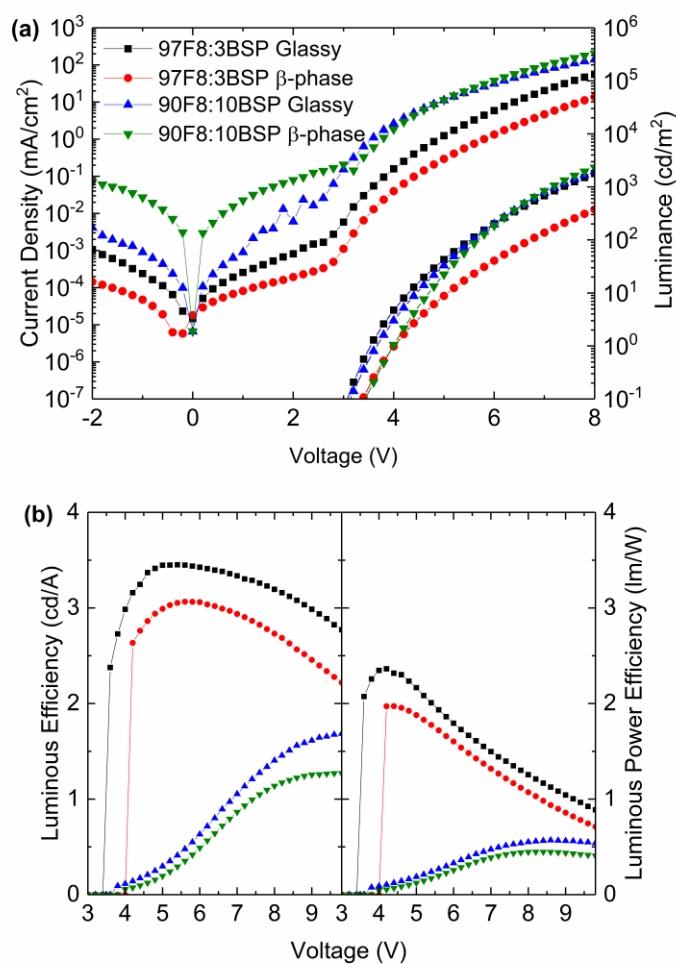


Figure S12. (a) J-V-L characteristics and (b) luminous and luminous power efficiencies for 97F8:3BSP and 90F8:10BSP copolymer PLEDs with glassy and β -phase emission layer (EML) microstructures. The device structures comprised ITO/PEDOT:PSS/TFB/copolymer EML/LiF/Ca/Al. Layer thicknesses are the same as those used in 95F8:5BSP copolymer devices, details of which are given in the experimental section of the main text.

Table S4. Summary of best PLED device performance data comprising 1 cd/m² turn-on (V), peak luminous efficiency (cd/A), peak power efficiency (lm/W) and CIE colour coordinates for 97F8:3BSP and 90F8:10BSP copolymer EMLs with glassy and β -phase microstructures.

EML Microstructure	EML copolymer	Turn on (V)	Peak Luminous efficiency (cd/A)	Peak Power efficiency (lm/W)	CIE (x, y)
Glassy	97F8:3BSP	3.6	3.4 @ 5.0 V	2.4 @ 4.2 V	(0.15, 0.17)
	90F8:10BSP	3.8	1.7 @ 9.8 V	0.6 @ 8.6 V	(0.15, 0.16)
β -phase	97F8:3BSP	4.0	3.1 @ 5.6 V	2.0 @ 4.4 V	(0.15, 0.13)
	90F8:10BSP	4.0	1.3 @ 9.6 V	0.4 @ 8.2 V	(0.15, 0.15)

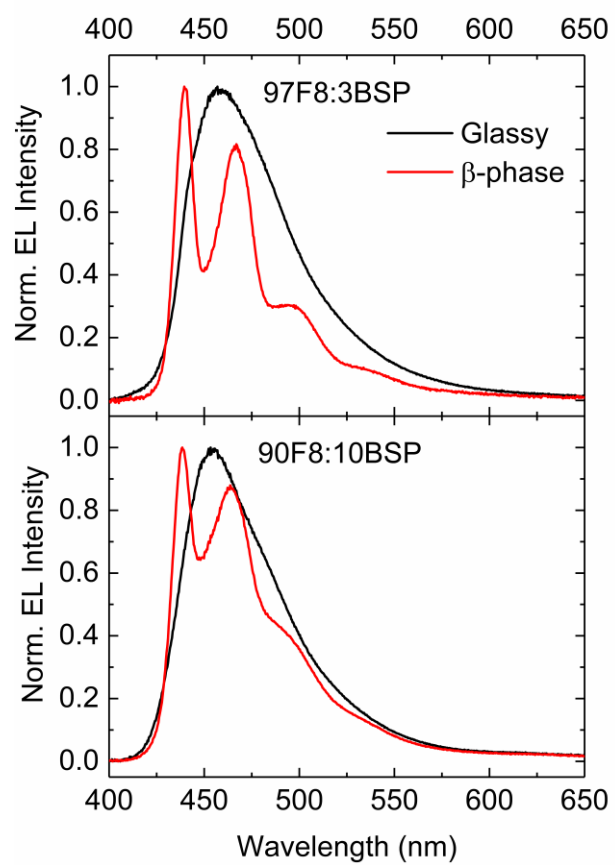


Figure S13. EL spectra for 97F8:3BSP and 90F8:10BSP copolymer PLEDs with glassy and β -phase EML microstructures.

95F8:5BSP PLED device lifetime

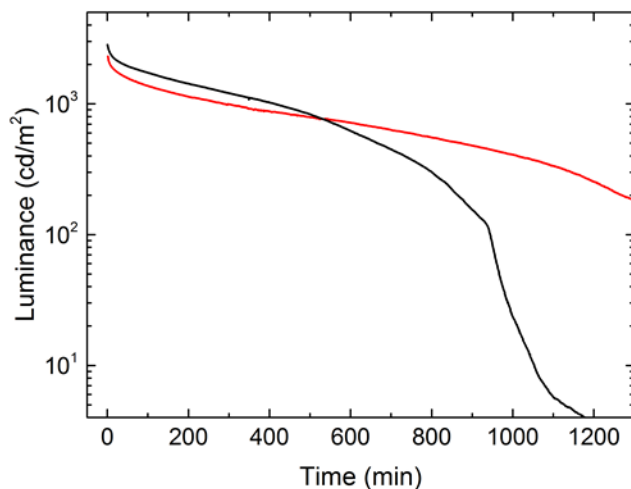


Figure S14. Accelerated luminance decay measurements for encapsulated 95F8:5BSP copolymer PLEDs driven at a constant current density $J \approx 90 \text{ mA/cm}^2$. Results are shown for both glassy (black line) and β -phase (red line) EML devices.

Both pre- and post-SVA 95F8:5BSP EML PLEDs were subjected to accelerated lifetime testing using a constant current source set to deliver 4 mA (i.e. $J \approx 90 \text{ mA/cm}^2$ for the 4.44 mm^2 pixels under test). The luminance was measured at 60-second intervals starting from 2821 cd/m^2 for glassy- and 2300 cd/m^2 for β -phase devices. Initially (Figure S15), the glassy and β -phase EML PLED luminance values decayed at a similar rate, with half decay times $T_{50\%}$ (glassy) = 176 mins and $T_{50\%}$ (β -phase) = 180 mins. The subsequent decay was much more rapid in the glassy copolymer EML devices, especially beyond 400 mins. The luminance took 490 mins to drop to 30% of its starting value for the glassy 95F8:5BSP EML PLED, but took 630 mins to reach the same fractional output for the β -phase device. In addition, whilst the latter was still emitting some 250 cd/m^2 at 1200 mins the glassy device luminance had fallen below 4 cd/m^2 by

that time. The operational stability of the β -phase 95F8:5BSP copolymer EML device is clearly significantly greater than for the corresponding glassy-phase device.

It is expected that the initial luminance decay is caused by degradation of the reactive LiF and Ca layers in the composite cathode that is used for both device types. The subsequent degradation is slower for the β -phase EML structures for which the emission is dominated by F8 centred excitonic states. In addition to the known stabilising effect of β -phase on extended F8 sequences,^{S5} this difference suggests a reduced stability for the BSP moiety centred CT like states that dominate emission from glassy copolymer EML structures.

In summary, therefore, induction of β -phase chain segments in 95F8:5BSP copolymer EMLs not only improves PLED CIE coordinates, but also operational lifetime.

Low temperature photoluminescence measurements

Figure S15 (a) shows that as the PFO β -phase sample decreases in temperature, the PL spectra red shifts by ~ 5 nm whilst the 0-0 linewidth decreases by some ~ 35 meV which has been previously linked to increases in β -phase conjugation length and planarity.^{S6} The 0-1 and 0-2 vibronics show distinctive splitting into at least three peaks. Figure S15(b) shows the glassy 95F8:5BSP copolymer emission reduces in linewidth as temperature decreases, with the spectra resolving into a main high energy peak at ~ 454 nm with a lower energy shoulder at ~ 478 nm. Low temperature β -phase 95F8:5BSP PL measurements (Figure S15(c) and (d)) reveal the spectra remains a superposition of both the vibronic β -phase emission and a CT-like emission from BSP centered states from 10–290 K. Spectral deconvolution reveals the component spectra appear identical to either the PFO β -phase or the glassy 95F8:5BSP spectra at each particular temperature, an example of which is shown in Figure S15(e) for 10 K. By integrating the component spectra at each temperature we find that (Figure S15(f)) the fraction of β -phase emission decreases as temperature decreases, from $\sim 64\%$ at 290 K to $\sim 32\%$ at 10 K.

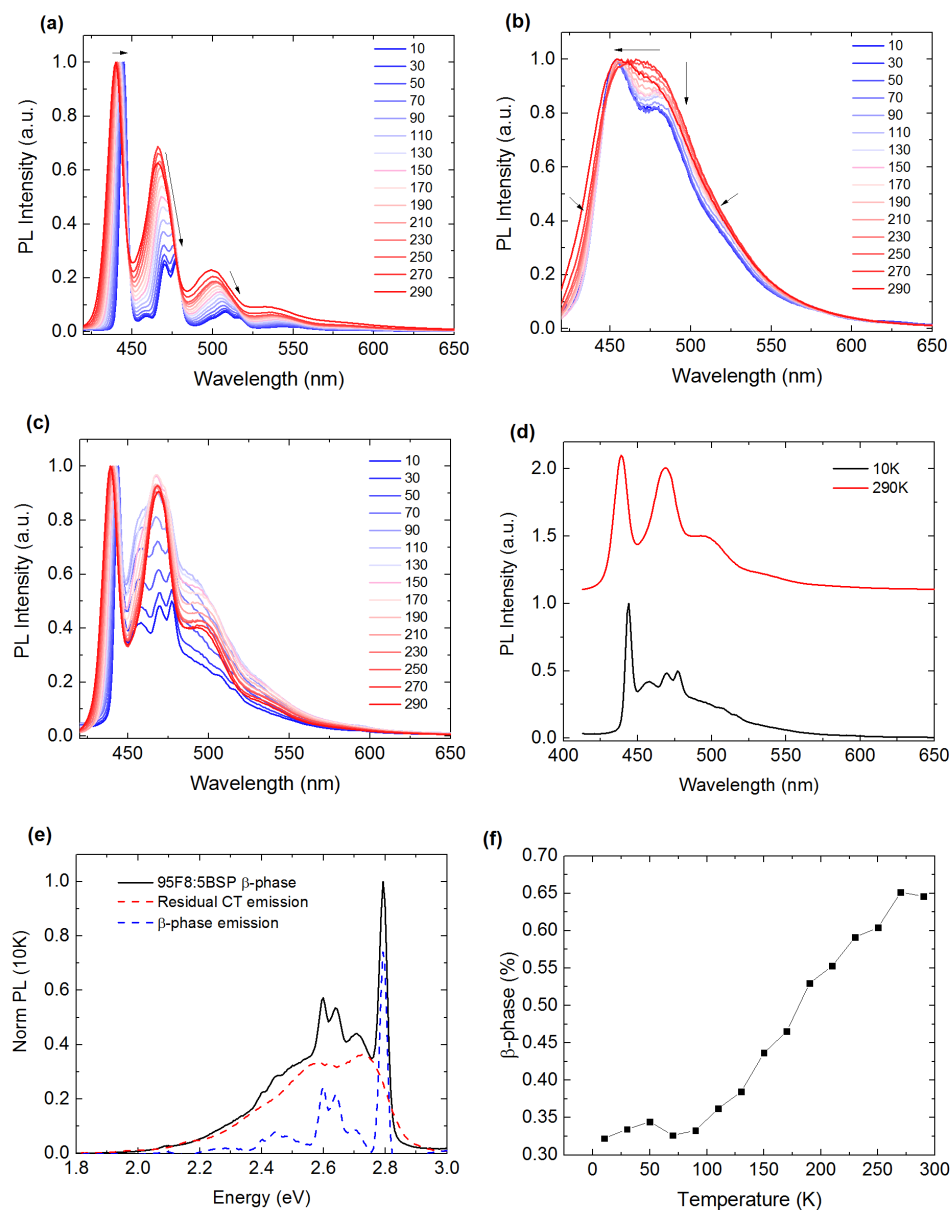


Figure S15. Photoluminescence spectra ($\lambda_{\text{ex}} = 400$ nm) of (a) β -phase PFO, (b) glassy phase 95F8:5BSP and (c) β -phase 95F8:5BSP samples at a temperature range of 10 to 290 K. Panel (d) shows the β -phase 95F8:5BSP spectra at 10 K and 290 K and (e) shows the deconvolution of the 10 K β -phase 95F8:5BSP spectra into the component β -phase and residual CT emission. Panel (f) shows the percentage fraction of β -phase emission as a function of temperature.

Voltage dependent EL spectra for a ~95 nm thick 95F8:5BSP β -phase PLED

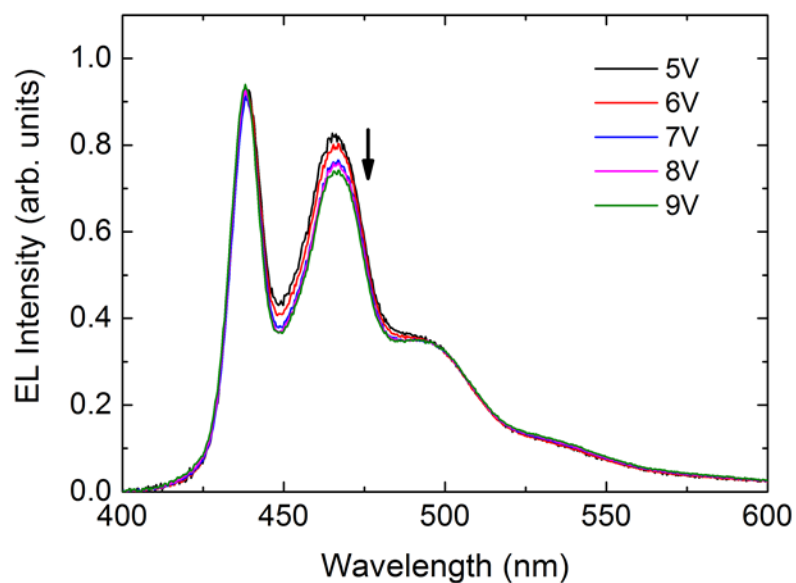


Figure S16. Voltage dependent EL spectra for a β -phase 95F8:5BSP PLED with an EML layer thickness of ~95 nm. The fraction of residual CT like emission appears to reduce with increasing voltage as BSP sites become saturated and β -phase F8 segments become filled with excited species. This can be seen by a reduction in intensity between 445-495 nm with increasing voltage.

Energy transfer mechanism in 90PFO/10PFB blend films and PLEDs

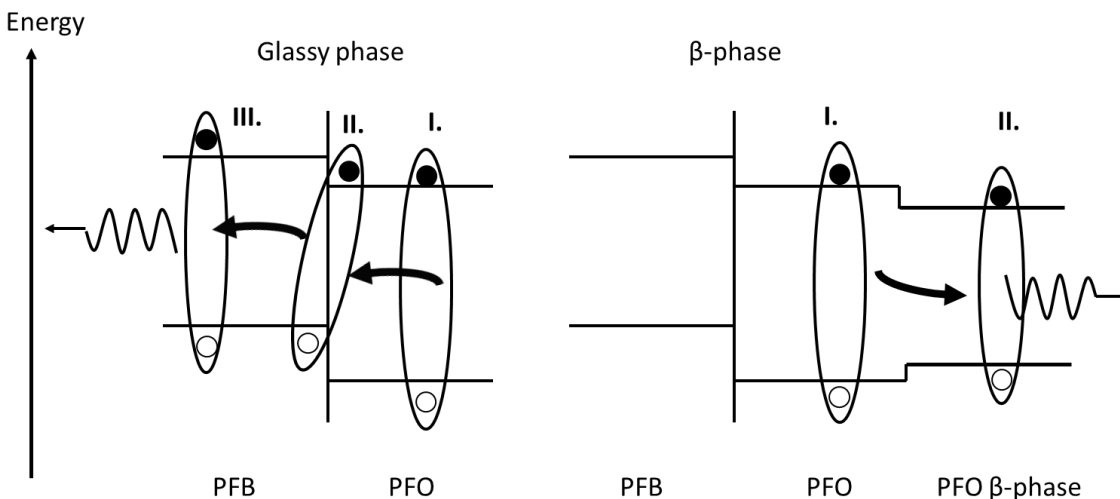


Figure S17. Diagram showing anticipated energy transfer in 90PFO/10PFB blend films after optical excitation of glassy PFO chain segments.

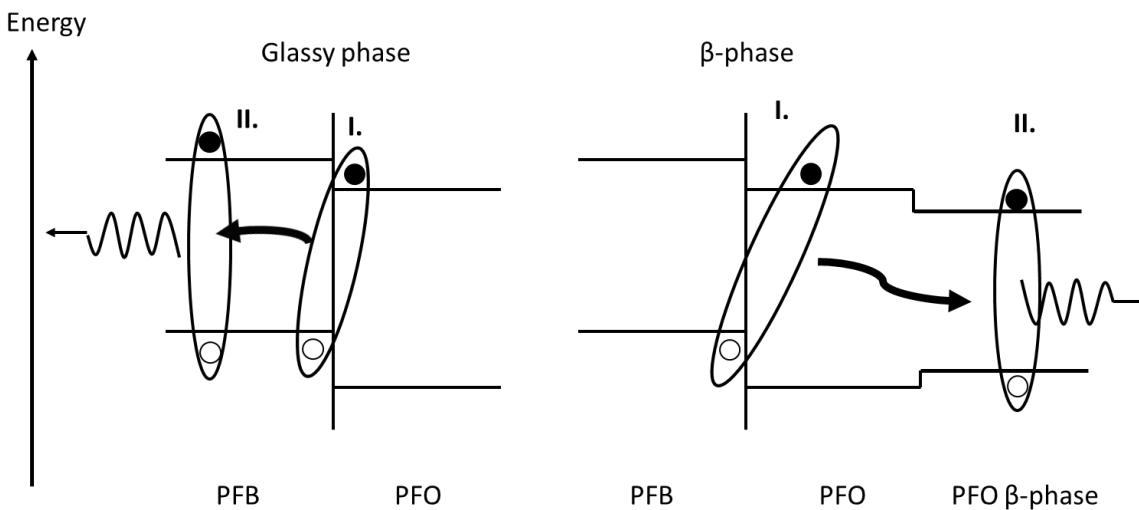


Figure S18. Diagram showing anticipated energy transfer mechanism in 90PFO/10PFB blend after electrical excitation forms a PFB:PFO exciplex state.

References

- (S1) Perevedentsev, A.; Chander, N.; Kim, J.-S.; Bradley, D. D. C. Spectroscopic Properties of poly(9,9-Dioctylfluorene) Thin Films Possessing Varied Fractions of β -Phase Chain Segments: Enhanced Photoluminescence Efficiency via Conformation Structuring. *J. Polym. Sci. Part B Polym. Phys.* **2016**, *54*, 1995–2006.
- (S2) Janietz, S.; Bradley, D. D. C.; Grell, M.; Giebeler, C.; Inbasekaran, M.; Woo, E. P. Electrochemical Determination of the Ionization Potential and Electron Affinity of poly(9,9-Dioctylfluorene). *Appl. Phys. Lett.* **1998**, *73* (17), 2453–2455.
- (S3) Sekine, C.; Tsubata, Y.; Yamada, T.; Kitano, M.; Doi, S. Recent Progress of High Performance Polymer OLED and OPV Materials for Organic Printed Electronics. *Sci. Technol. Adv. Mater.* **2014**, *15* (3), 34203.
- (S4) Chan, K. L.; Sims, M.; Pascu, S. I.; Ariu, M.; Holmes, A. B.; Bradley, D. D. C. Understanding the Nature of the States Responsible for the Green Emission in Oxidized poly(9,9-Dialkylfluorene)s: Photophysics and Structural Studies of Linear Dialkylfluorene/fluorenone Model Compounds. *Adv. Funct. Mater.* **2009**, *19* (13), 2147–2154.
- (S5) Arredondo, B.; Romero, B.; Gutiérrez-Llorente, A.; Martínez, A. I.; Álvarez, A. L.; Quintana, X.; Otón, J. M. On the Electrical Degradation and Green Band Formation in α -And β -Phase poly(9,9-Dioctylfluorene) Polymer Light-Emitting Diodes. *Solid. State. Electron.* **2011**, *61* (1), 46–52.
- (S6) Ariu, M.; Sims, M.; Rahn, M. D.; Hill, J.; Fox, A. M.; Lidzey, D. G.; Oda, M.; Cabanillas-Gonzalez, J.; Bradley, D. D. C. Exciton Migration in β -Phase poly(9,9-Dioctylfluorene). *Phys. Rev. B* **2003**, *67* (19), 195333.